CHALMERS
UNIVERSITY OF TECHNOLOGY

Design Evaluations of IKEA Friction hinge

Master's thesis in Product Development

Dominika Hamulczuk
Shyam Chafekar

DEPARTMENT OF MECHANICS AND MARITIME SCIENCES

CHALMERS UNIVERSITY OF TECHNOLOGY
Gothenburg, Sweden 2021
www.chalmers.se

Design Evaluations of IKEA friction hinge
DOMINIKA HAMULCZUK
SHYAM CHAFEKAR

Master's thesis 2021:42
Department of Mechanics and Maritime Sciences
Chalmers University of Technology
SE-412 96 Göteborg
Sweden
Telephone: +46 (0)31-772 1000

Cover:
Dismantled assembly of a friction hinge. Photograph by Shyam Chafekar

Chalmers Reproservice
Göteborg, Sweden 2021

Design Evaluations of IKEA friction hinge
Master's thesis in Product Development
DOMINIKA HAMULCZUK
SHYAM CHAFEKAR
Department of Mechanics and Maritime Sciences
Chalmers University of Technology

Abstract

The goal of this master thesis conducted with IKEA was to better understand the friction hinge technology and advance IKEA's development effort in this direction, based on the initial design of the hinge provided by them. Research questions to be answered were, among others, what are different types of such hinges, how to predict the torque produced, and which parameters influence the torque. The aim of the study was achieved by performing a mix of theoretical background studies, patent study, Finite Element Analyses, and experimental studies on physical prototypes. The Finite Element Analysis, done using ANSYS Workbench, was the main part of the project and included establishing 2D and 3D static structural models and performing simulations on them. The models were then calibrated and validated against the experimental data.

The numerical models reflected the reality well with an error of less than 20% in most analyzed cases. However, the experimental results had a high variance and did not correspond to expected boundary conditions. Optimization of the models allowed to reduce the simulation times to several minutes for 2D and 3-5 hours for 3D simulations while maintaining roughly the same quality of the results. Computationally inexpensive models made it possible to observe how the results change after altering some of the parameters. The studies on the numerical model showed that the interference depth is for such geometry not as crucial as the thickness of the part on shaft and coefficient of friction. Nevertheless, the high variance in the experimental study proved, that the problem is much more complex than expected and there are more factors in the design-manufacturing-assembly chain that influence the torque. That implies that a high factor of safety is needed for the product to be safe and reliable.

Keywords: Friction hinge, Finite Element Method, experimental testing, pattern study

Acknowledgements

First and foremost we thank Chalmers University of Technology and IKEA Sweden for giving us the opportunity to work on this project.

We would like to thank our company supervisors, Katarzyna Kierska and Magnus Månsson for their continuous guidance and support throughout the project. Your energy and knowledge allowed us to move forward with the project and continue making progress despite the cold Swedish winter weather.

We thank our supervisor and examiner Jim Brouzoulis for his guidance and support. Your insights were invaluable and helped us overcome obstacles encountered on our way.

We would additionally like to thank Björn Stoltz for his valuable inputs to the project. Your knowledge, experience, and great attention to detail helped us become meticulous in our work.

We also thank Xabier Aginagalde for his time and effort dedicated to this project. Lastly, we would like to thank our friends and families for their love and unending support.

Nomenclature

CW - Clockwise
CCW - Counter clockwise
FEM - Finite element method
FMEA - Failure mode and effects analysis
FOS - Factor of safety
HSS - High speed steel
ID - Inner diameter
OD - Outer diameter
POS - Part on shaft
THK - Thickness

Due to IP restrictions geometric data has been hidden in this version of the report. The geometric data has been replaced by abbreviations of the physical parameters, for example THK A, would represent the thickness value.

Contents

1 Introduction

Friction hinges are a type of joint that facilitates a pivot with a certain amount of resistance to the motion. Instead of allowing the pivoting object to swing freely, the friction hinge slows down the movement and/or allows for a complete halt of the object in the desired position. Friction hinges are usually used for safety (preventing too quick/accidental opening and closing of door elements) or for convenience (for example the ones used for laptop screens or in-home appliances equipment.

Friction hinges have been around for over a hundred years, with patents recorded as early as 1904 [25]. They have been used in various applications, such as boat hatches, furniture, electronic appliances, etc. IKEA wishes to use these in their home furnishing range. They believe this component can help extend their home furnishing range to meet the latest customer needs and demands.

The vision of IKEA is *to create a better everyday life for the many people* [15], and one of the core values is cost-consciousness [16]. The friction hinge is an example of one such technology that will align with this vision. It is a simple and cheap solution for safe and controlled pivoting of door elements. The addition of this technology will allow for efficient designs which will help lower the overall cost of the product.

IKEA plans to introduce a table that will serve two purposes in one product: a desk and a big dinner table. The furniture will have a hinged tabletop that can open and close based on the size requirement. The friction hinge will prevent the table from opening and closing rapidly making the table safer to use for the customer and reducing dynamic stresses on the table interfaces, hence increasing the life of the product and reducing the overall required strength.

Currently, IKEA does not offer friction hinges in its range and wishes to build on the knowledge required to add them to their offering. Furthermore, the goal is to create a better open and close experience for as many people as possible, so it is important to make the friction hinge affordable to be included in their lower-price range furniture. This was the driving force for developing knowledge about it throughout this thesis project.

Since this thesis has been carried out in collaboration with IKEA, some business sensitive information has been censored from this version of the thesis and replaced with non-numerical values (THK for thickness values, ID for inner diameter of the part on shaft, OD for outer diameter of the shaft, INT for interference). Geometric data which could potentially be business critical has been hidden due to IP restrictions. If the geometric data is made public it can help business competitors develop similar friction hinge using the data provided in this report.

1.1 Background

Before the thesis project, IKEA carried out some development work on the friction hinge. They identified a requirement for the friction hinge and performed a cost evaluation. Since the cost of acquiring these hinges through an external supplier was high, the possibility of sourcing friction hinges internally was explored. Based on the requirements, a friction hinge design that was not patent protected was selected and a few samples of this hinge were produced using IKEA's internal supplier. The details of the initial samples are described in Section 4.3. From the tests performed on these prototypes, it was seen that the hinge design did not perform as expected. The torque values were not as per the predictions and the hinges did not have adequate product life in comparison to the requirements. It must also be noted that the parts were not manufactured at production specifications but were prototypes.

1.2 Aim of the study

This study was carried out to better understand the design of friction hinge. To keep costs under control, IKEA wants to manufacture the friction hinge through their internal suppliers, and in order to do this, the company needs the knowledge of how to design the friction hinge for various requirements. Which parameters influence the hinge torque and life. Finally, the relationship between them must be examined. This will allow IKEA to control the design as required. This study aimed to understand friction hinge technology to date, hence a thorough literature and patent study were needed.

The current IKEA hinge is designed with a particular geometry, a question mark shaped sleeve that slides onto a cylindrical shaft with an interference fit. As a start point for the thesis it is important to understand

the possibility of having a hand calculations model to predict the torque behavior of this geometry and validate the numerical model.

During the initial development of the hinge, there were several unanswered problems described in Chapter 2. This project aimed to tackle some of these issues and find the answers that will help future development efforts.

1.3 Challenges in the design

The hinge function is primarily dependent on the interference fit between the parts. The geometry of the interfering members makes it difficult to analytically predict the exact expansion and contact pressure it would exert on the shaft. It is important to be able to predict the contact pressure between the shaft and the parts on the shaft with high accuracy to calculate the friction, as it directly affects the torque required to operate the hinge. This information will be invaluable when developing further hinges for various requirements.

As described in Chapter 2, two complete samples were produced, which provides few data points to serve as preliminary validation data for the FEM model. However, to be confident the numerical model provides fairly accurate torque values, an additional number of data points were needed. The accuracy and validity of the experimental setup used to measure the torque in the prototype sample was another point of concern. Hence it was important to design an appropriate test to determine the torque required to rotate the shaft.

1.4 Methodology

This thesis project was divided into three main stages: a theoretical study, Finite Element Analysis, and experiments on prototypes. The first stage involved carrying out a literature and patent study. This allowed us to determine and investigate current technologies and active patents in the field to identify research that is already conducted on this topic. The study also involved a market analysis to understand the current market trends. The findings from this study together with the attempts to establish a hand calculation model are described in Chapter 3.

A FEM model, developed during the second stage, was used to determine the contact pressure and the torque required to rotate the hinge. The development of the FEM model was the largest task carried out in the project. Chapter 5 explains the process and presents results from the models. The methodology for establishing the FEM model consists of 3 steps, Verification, Calibration, and Validation.

- Verification stage: To ensure that the model behaves realistically, to check from an engineering judgment that there is no irregular behavior to the model.
- Calibration: To match the model against a sample data points from the empirical data.
- Validation: Compare the results from the FEM model against a different set of experiments, identify errors and deviations from the experimental data.

The validation step overlaps with the third stage, where the torque measuring experiment is designed and carried out to collect a large and reliable set of data.

2 IKEA's development efforts

This chapter explains in detail the friction hinge design used at IKEA. It includes the description of the development work carried out on the hinge prior the start of this thesis project. The application for which the hinge is being designed and the current requirements are also listed in the chapter.

2.1 Physical Construction

The hinge is made up of 8 unique parts and the assembly is shown in Figure 2.1. The details of the parts are as listed in Table 2.1.

sl.no	Part	Final material spec	Prototype material
1	Right_Part_round	Die cast zinc alloy (ZAMAK)	Aluminium alloy (AlSi10Mg)
2	Spacer	Polyoxymethaline(POM)	POM
3	Part on Shaft (POS)	Stainless steel 316L (Cold formed)	Stainless steel 316L (3D printed)
4	Shaft	High speed steel	High speed steel
5	Mid_Part_round	Die cast zinc alloy (ZAMAK)	Aluminium alloy (AlSi10Mg)
6	O-ring	Rubber	Rubber
7	Left_Part_Round	Die cast zinc alloy (ZAMAK)	Aluminium alloy (AlSi10Mg)

Table 2.1: Bill of materials of the hinge.

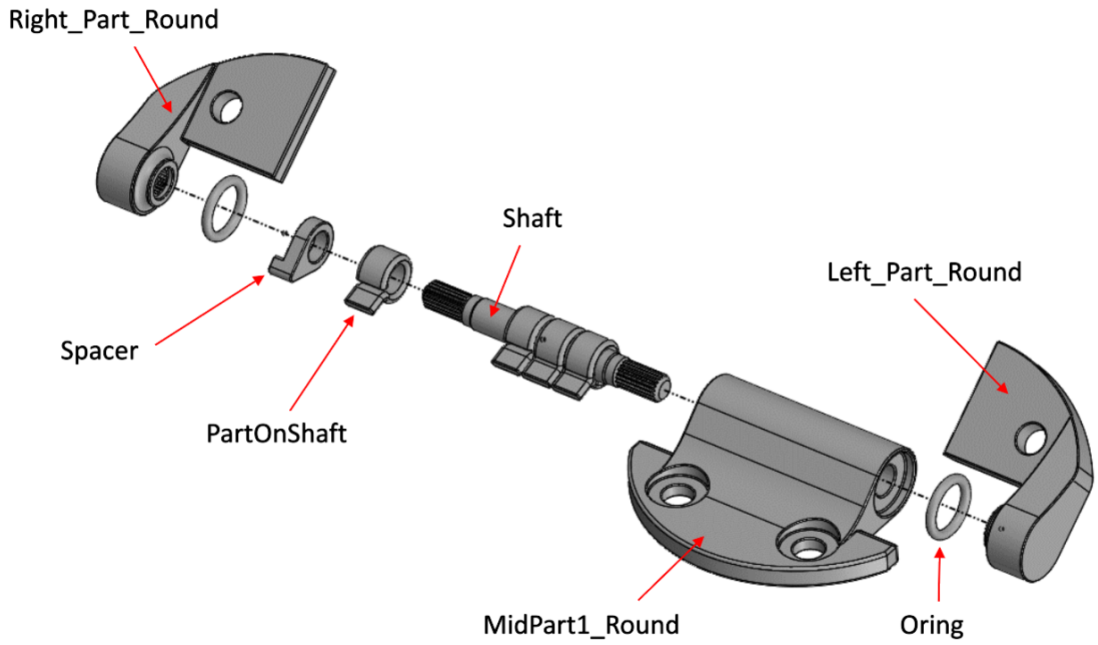

Figure 2.1: *Exploded assembly of the hinge.*

2.2 Hinge application

The preliminary application for the hinge is a foldable table. The table will consist of two boards joined together by the hinge. This will allow the user to change the size of the table top by simply folding or unfolding the table in half. The friction hinge will be used on account of user safety and to reduce the loads on the joints

when the table is opened/closed. Since the hinge will slow down the movement of the table top, the stresses the joints need to endure during opening and closing is lower due to lower kinetic energy, thus allowing a more slender construction at the joints. The specifications of the table are:

Parameter	Value
Dimensions	118 cm X 40 cm X 2 cm
Weight	2.8 kg
Material	Wood

Table 2.2: Table specifications.

2.3 Requirements

Based on the application, the requirements for the hinge were formulated by IKEA. They are listed in the Table 2.3. However, not all of them are of concern for this project (e.g. requirements 5-10).

	Category	Requirement	Value
1	Performance	Hinge mechanism shall support the table top in place under the influence of the table's own mass.	2.8 kg
2	Performance	Within 50 mm of the full closed position and 50 mm of the full open position, the table top shall not drop more than 12 mm (Figure 2.2a).	12 mm
3	Performance	Torque required to open/close the hinge.	3.4 Nm +- 10%
4	Durability	Minimum number of the open & close test cycles the hinge must survive without any loss of integrity.	5,500 cycles
5	Interface	The hinge shall not protrude more than the value above the table top (Figure 2.2b).	0.3 mm
6	Interface	The maximum diameter of the hinge at the fulcrum (Figure 2.2b).	7 mm
7	Interface	The maximum gap between the two table tops in fully opened position (Figure 2.2b).	1 mm
8	Interface	Shape of cut.	Round
9	Interface	Cut diameter.	56.5 mm
10	Interface	Cut depth.	6.2 mm

Table 2.3: Requirement list.

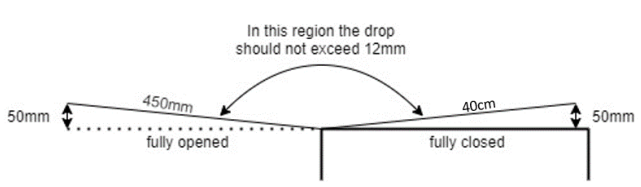

(a) *Diagram illustrating requirement 2*

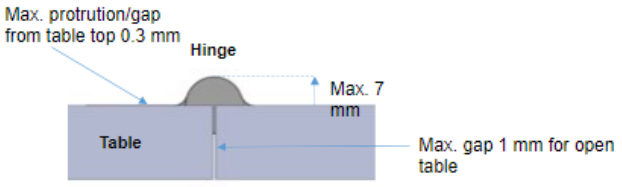

(b) *Diagram illustrating requirements 5-7*

Figure 2.2: *Illustrations of some of the requirements*

2.4 Initial tests

The first samples of the shaft and parts of shaft (POS) were produced by the supplier to examine the torque characteristics in relation to the interference. Results of the initial tests are presented in Table 2.4.

POS Material	sl.no	Interference(mm)	CCW	CW
INOX	1	INT C	0.6 Nm	0.3 Nm
	2	INT B	0.5 Nm	0.25 Nm
	3	INT A	0.45 Nm	0.25 Nm
PKT-117	1	INT C	1.5 Nm	0.9 Nm
	2	INT B	1.2 Nm	0.85 Nm
	3	INT A	1.7 Nm	1.15 Nm

Table 2.4: Interference test performed by the supplier for increasing interference.

Tests were also carried out to determine the influence of lubrication on the torque characteristics. A layer of teflon based lubricant was applied on the shaft and the POS separately. The findings are shown in Table 2.5.

Test	sl.no	Interference(mm)	Direction1	Direction2
No lubricant	1	INT C	0.75 Nm	0.5 Nm
	2	INT B	0.9 Nm	0.6 Nm
	3	INT A	1.15 Nm	0.7 Nm
Lubricant on POS	1	INT C	0.8 Nm	0.5 Nm
	2	INT B	0.8 Nm	0.55 Nm
	3	INT A	1.15 Nm	0.75 Nm
Lubricant on shaft	1	INT C	0.7 Nm	0.45 Nm
	2	INT B	0.75 Nm	0.55 Nm
	3	INT A	0.9 Nm	0.5 Nm

Table 2.5: Lubrication test performed by the supplier for increasing interference.

The addition of lubricant reduced the torque slightly, but when compared the variation in torque values seen in the experimental study performed later in this project, the change due lubrication is insignificant. Hence it was determined that lubrication will not play a big role in the final torque offered by the hinge. Lubrication, however, will be necessary to minimize wear of the POS and shaft.

The tests, so far, were conducted for single parts on shaft assembled onto the shaft. The next tests were conducted with multiple POS assembled onto the shaft. Two full hinge assemblies (shaft, parts on shaft and casing) were also built to test the complete product. The assembly patterns of the hinges are shown in Figure 2.3 and the results of this test are shown in Table 2.6. It can be observed that the measured torque does not increase in the expected pattern i.e the torque from two POS is not exactly double of the torque of a single POS. To explain this phenomenon was considered as one of the research questions for the thesis.

Sample no	Test no	CCW rotation	CW rotation
Sample 1	1	0.85 Nm	0.4 Nm
	2	1.85 Nm	1.35 Nm
	3	3 Nm	2 Nm
	4	4 Nm	3.3 Nm
Sample 2	1	0.8 Nm	0.45 Nm
	2	1.75 Nm	1.25 Nm
	3	2,75 Nm	1.75 Nm
	4	3.45 Nm	2.65 Nm

Table 2.6: Results from fully assembled sample.

Other components of the hinge such as middle part and right and left part were 3D printed using a direct laser metal sintering process. The shaft was machined in a CNC lathe, and the POS were manufactured with stamping process. The complete assembled samples are shown in Figure 2.4. These samples were assembled on

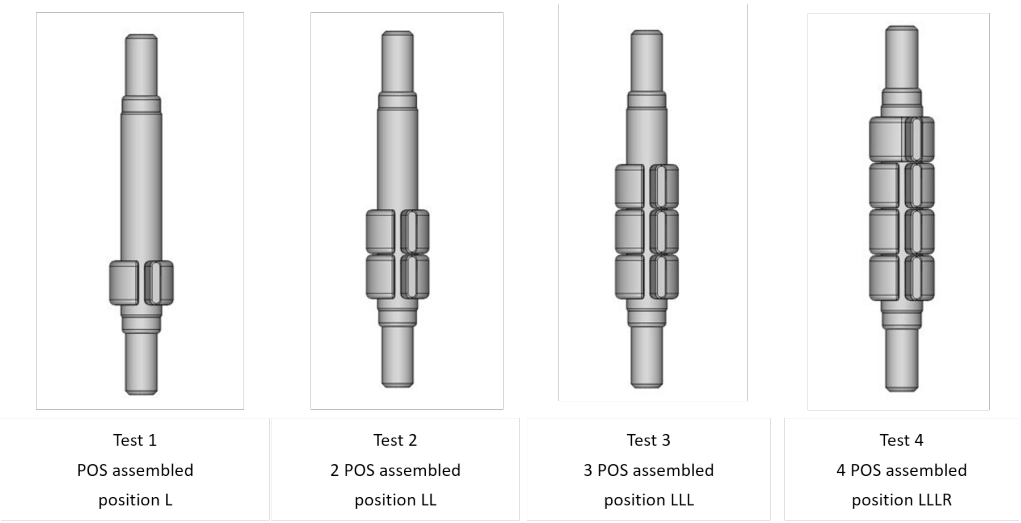

Figure 2.3: *Assembly positions of POS. The test was performed to check how adding consecutive parts on shaft will influence the torque.*

a table setup and used for a lifecycle analysis. Opening and closing of the hinge multiple times was simulated, the durability requirement being 5,500 cycles, but it was seen that the hinge failed before reaching this value. The failure points of the hinges have been captured in Figure 2.5. The failure A is a loss of integrity of the middle part and the failure B is a failure of the splines. Both these failures would mean the hinge cannot continue function without damaging the product or the user. The causes for these failures are explored in the Failure Mode and Effects Analysis (FMEA) shown in Section 2.6.

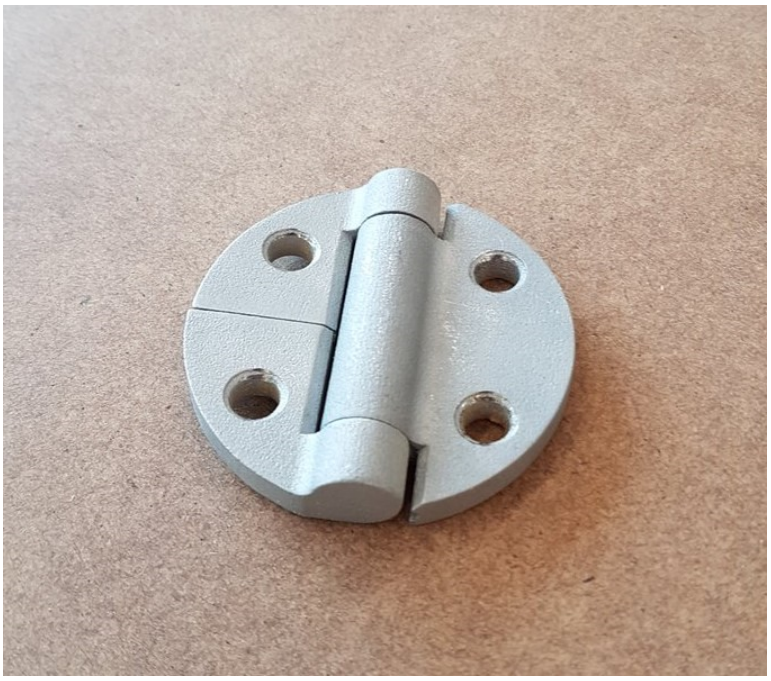

Figure 2.4: *Assembled hinge.*

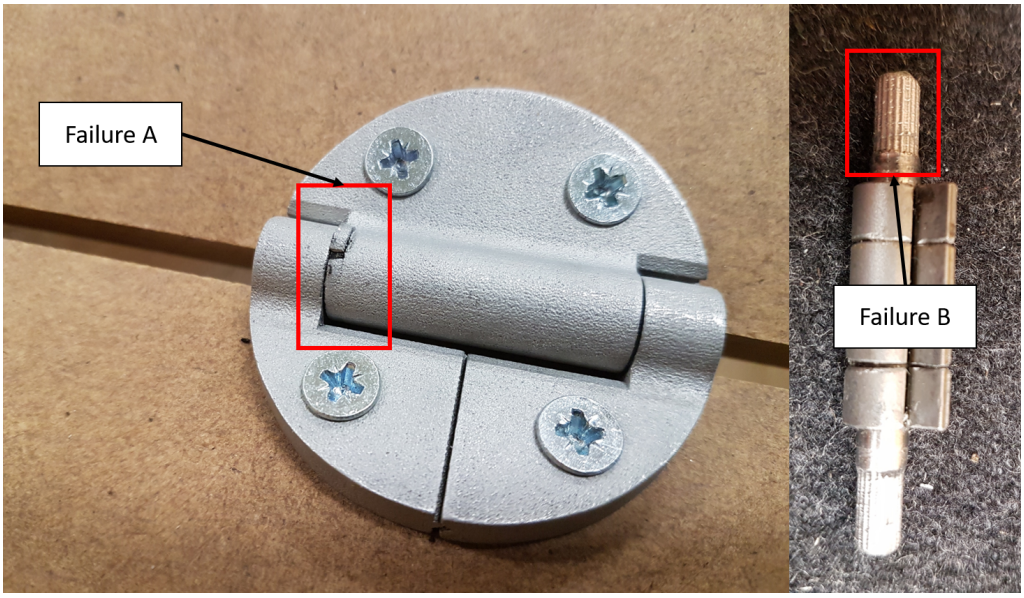

Figure 2.5: *Hinge failure points.*

2.5 Measurement method

To measure the torque, the suppliers for IKEA used an iterative method as seen in Figure 2.6. A torque screwdriver was set to particular torque and used on the shaft to see if the torque is high enough to rotate the shaft. This method however was dependent on the skill of the user to ensure that there are no undesired forces applied to the sample. The applied torque, on the device, needed to be readjusted after every measurement, which was not only a tedious work, but it reduces the resolution of measurement. The uneven torque values seen on the results for the sample prototypes raises the question of accuracy of the torque measurement method. A mitigation for this problem is presented in Section 4.3.1.

Figure 2.6: *Torque measurement method.*

2.6 Failure mode and effect analysis

A failure mode and effects analysis is conducted based on the data from the initial tests and observations (Appendix A). The goal of the study was to analyze each part of the hinge and identify their failure modes as well as the potential resulting effects on the rest of the system. Control methods that may help detecting and preventing the failure to be applied during the design process were also listed.

3 Literature Review

This chapter describes the theoretical background of the friction hinge. First, the friction hinge types and technologies are described with a commercial example of each hinge type. Next, the findings from the patent study are presented followed by the theoretical calculations of the interference fit assuming two closed rings and a 1D axisymmetric case.

3.1 Friction hinge types and technologies

Friction hinges come in various shapes and sizes and are based on various technologies. Depending on which one of the varieties of application of the hinge will be used for, the torque provided ranges from tenths of 1 Nm up to 11 Nm. Though the friction hinge market is quite large with several different companies from all around the world manufacturing such devices, nearly all of the hinges are based on one of five technologies. These technologies are roll pin, torque disc, tapered shaft, question mark band, and clip hinges [30].

3.1.1 Roll pin or barrel hinge

Roll pin or barrel hinge is the simplest friction hinge mechanism. Figure 3.1a presents the schematics of such hinge. In the basic configuration, the hinge comprises three elements: two leaves and a pin. Before assembly, the diameter of the leaf knuckles is smaller than the shaft diameter. That way when the hinge is assembled, the interference fit between the leaves and pin induces contact pressure which in turn causes torque during relative movement of the knuckles and the shaft.

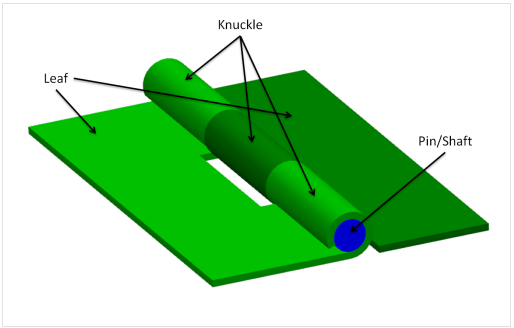

(a) *Roll pin hinge.*

(b) *Adjustable friction hinge (FH010SS hinge by Sierra Pacific Engineering & Products [32]).*

Figure 3.1: *Examples of roll pin hinges.*

The same kind of hinge can also be created in a way that allows for adjustable torque. The hinge is then usually composed of two knuckles, where the free end of the inner one is attached to the leaf by a screw. Figure 3.1b presents an example of such adjustable barrel hinge.

3.1.2 Torque disc hinge

In a torque disc hinge, friction is induced between the two hinge leaves rather than between the leaf and the shaft. The leaves are press against each other with a spring washer and a screw. This kind of hinges usually has an adjustable torque. Figure 3.2 presents the schematic picture of such hinge and the HG-TA45R product by Sugatsune [34] that uses this technology.

3.1.3 Tapered shaft hinge

Another type of easily adjustable hinge is a tapered shaft hinge. An example of such is CMUF-SR hinge by Elesa [6] (Figure 3.3b). Here, both the shaft and one of the middle knuckles have a conical shape. This means,

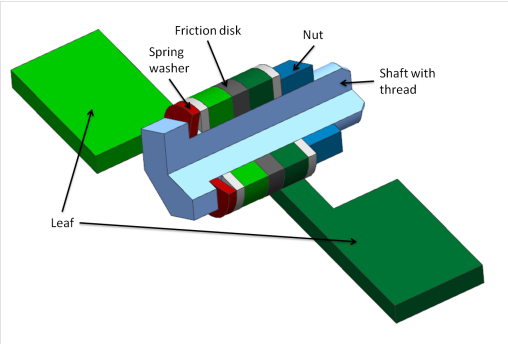

(a) *A schematics of a friction disc hinge.*

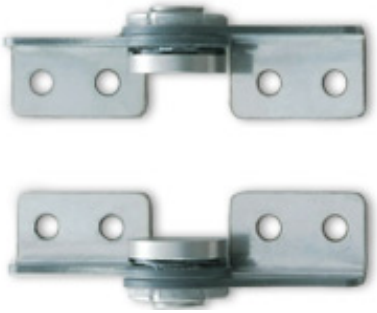

(b) *HG-TA45R hinge by Sugatsune [34].*

Figure 3.2: *Examples of friction disk hinges.*

that as they are pressed against each other (e.g. by tightening the screw on the end of the shaft), the friction between them increases.

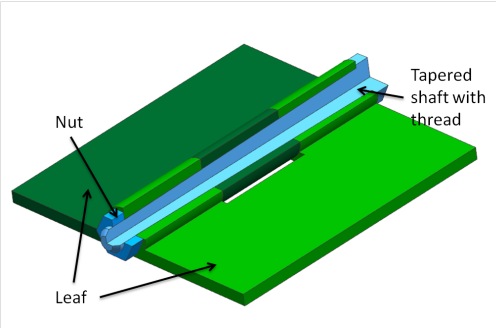

(a) *A schematics of a tapered shaft hinge.*

(b) *CMUF-SR hinge by Elesa [6].*

Figure 3.3: *Examples of tapered shaft hinges.*

3.1.4 Question mark band hinge

The question mark band hinge, as shown in Figure 3.4, is a modular component with one or more question mark-shaped members with the inner diameter in the relaxed state smaller than the diameter of the shaft. That way when assembled on the shaft there is an interference fit between the members and the shaft which causes friction. The elongated part of the members slides in a grove in the middle knuckle so that the rotation between the members and the leaf is restricted. The shaft on both ends is connected to the two other leaves using a spline or polygon connection. Due to the unsymmetrical shape of the members, the torque generated in the clockwise direction is different from the one generated in the anticlockwise direction.

3.1.5 Clip hinge

Clip hinges in principle work the same as the question mark band hinges with the only difference being the shape of the parts on the shaft (Figure 3.5). The c-shaped clips are symmetrical, so the torque is the same regardless of the turning direction.

3.2 Patent study

In this section, the patent study on the topic of the fiction hinge is described. The goals of the study were to identify possible active patents that may be infringed upon by the design under development during the master

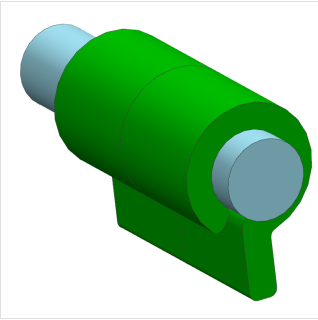

(a) *A schematics of a question mark band hinge.*

(b) *Fixed Position Hinge by Essentra Components [7].*

Figure 3.4: *Examples of question mark band hinge.*

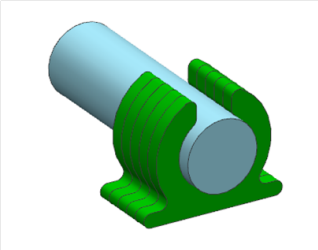

(a) *A schematics of a clip friction hinge.*

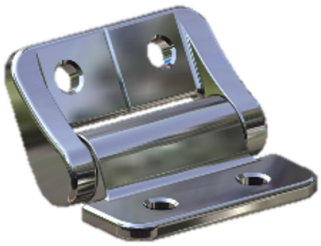

(b) *PHCS hinge by Reel Precision Manufacturing [34].*

Figure 3.5: *Examples of clip friction hinges.*

thesis project and to gain more knowledge about the prior art, which are any type of information regarding the invention already known to the public [9]. Both of these aspects were considered equally important. Identifying active patents in the same technological area is crucial to avoid wasting time on the design that is already existing and protected by patent laws. Prior art study, on the other hand, allows to broaden the knowledge regarding the technology, distinguish the issues that the component may suffer from, and avoid duplication of research efforts.

The patent search was conducted with the focus on question mark band and clip hinges. The search was done using *Google patents* [13] and European Patent Office's search engine *Espacenet* [8] using key words and Boolean expressions (e.g. "hinge" AND ("tilt" OR "friction" OR "torque")), assignees (e.g. Reell Corporation), and citations.

3.2.1 Active patents in the area

No active patents similar to the studied design, used as the basis in this project, were identified. The question mark band design as used in this project was listed as a "prior art" in the patents number US5491874A [23] and WO9503464A1 [12], both from 1993, which suggests that the technology is in the public domain. The c-shaped clips patented first by the Reell Corporation in 1995 [11] are also in the public domain as in their basic version (shaft + clips). However, in the years following the publication of these patents, several improvements for these designs were created and filed for patent protection, though not all of them were given the patent for various reasons. The next subsection will cover these publications and designs.

3.2.2 Market trend and identified issues

The patent study has shown that there exists a research effort directed mostly towards clip and band hinges. Three main directions of the research were identified: improvement of c-shaped clips, improvement of question mark-shaped clips, and the improvement of the closed profile clips.

Question mark hinge

This design is older than the other two types of friction hinge. The earliest identified patents on the question mark hinge technology come from 1993, and they were already stating the basic design as prior art and introducing improvements. This implies that the technology is quite old. Two very interesting patents on this subject are US5491874A [23] and US5950281A [24]. The first one proposes the solution for the phenomenon of uneven distribution of pressure in the hinge by adding groves on the inner side of the clip that can double as lubricant reservoirs (Figure 3.6). The latter one proposes the design of the clip that for a part of its width has the slit on the opposite side for more even torque in clockwise and anticlockwise directions (Figure 3.7).

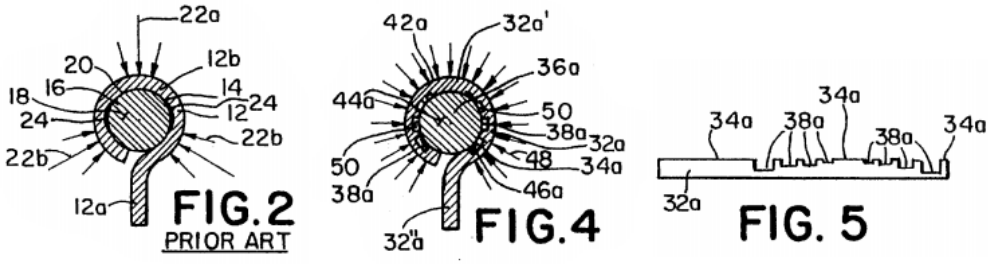

Figure 3.6: *A drawing from the US5491874A patent [23]. The groves on the bottom of inner side of the clip allow for even distribution of the pressure on the shaft.*

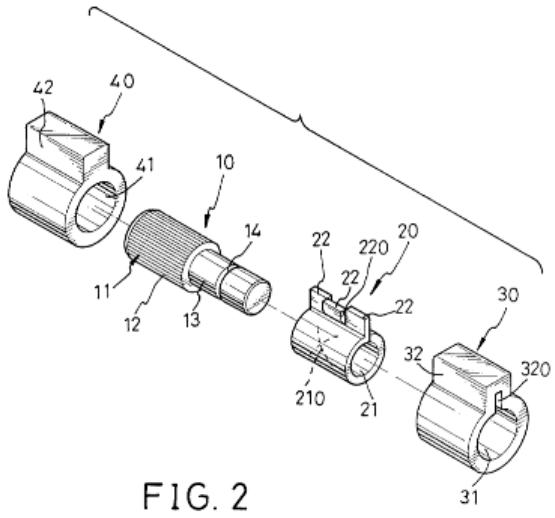

Figure 3.7: *A drawing from the US5950281A patent [24]. The shape of the clip helps to obtain equal torque in both turning directions.*

C-shaped clips

This design was proposed by Reell Corporation in 1995 [11]. Since then the company filed for two more patents that use the same technology, gradually improving the design [35][20] (Figure 3.8). Both patents added the solutions for housings and assembly as improvements. The 2011 patent US2011232032A1 [3] (Figure 3.9) issued by Shin Zu Shing Co. Ltd introduces an additional hole in the clip whose role is to dissipate the internal stresses in the element. This suggests that stress concentration may be a problem worth looking into.

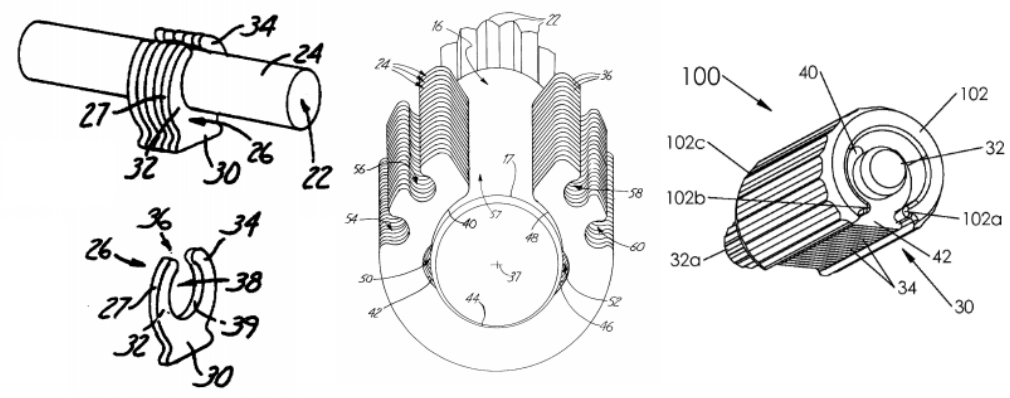

Figure 3.8: *The evolution of the Reell Corporation c-shaped clip hinge [35][20].*

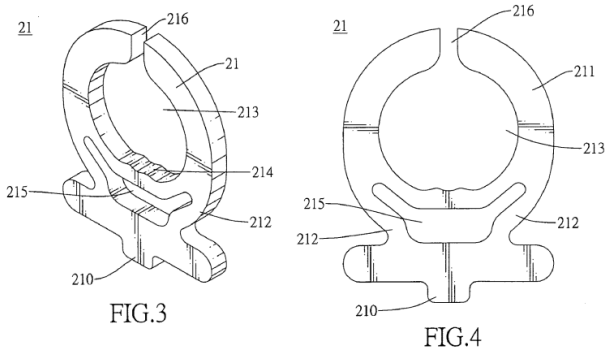

Figure 3.9: *Shin Zu Shing Co. Ltd patent that introduces a hole (215) in the clip (21) to dissipate stresses. [3]*

Closed profile clips

The closed profile clips have various shapes, but in the principle, it is a disk with the inner hole of the shape that for part of the circumference has an interference fit with the shaft, while the rest of the profile allows the clip to deform slightly to reduce internal stresses [1][22]. Examples of such designs can be seen in Figures 3.10 and 3.11.

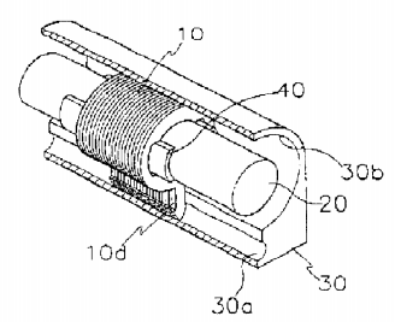

Figure 3.10: *US Patent 6467129B1 [1]. The pressure on the shaft is induced by two plate springs (40) placed in the grooves in the clips (10) along the shaft (20).*

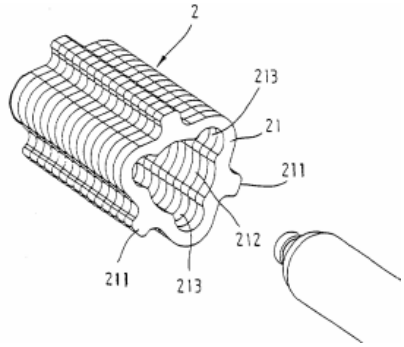

Figure 3.11: *US Patent 20020144378A1 [22]. Subholes (213) in the triangular clips increase its flexibility and can be used as a lubrication storage.*

3.3 1D axisymetric model

The interference fit is a fit between the hole and shaft where the minimum allowable diameter of the shaft is larger than the maximum allowable diameter of the hole. It always results in the interface between the shaft and the hub [19], hence assembly requires applying pressure, heating, or cooling. Due to the interference, during the assembly, both parts slightly deform creating a high contact pressure which in turn results in high friction.

For two concentric rings assembled with interference fit, the contact pressure can be calculated as a superposition of two axisymmetric thick-walled cylinders (Figure 3.12 [29]. Before the assembly, the outer radius of the inner cylinder is equal to b_{in}, while the inner radius of the outer cylinder is equal to b_{out}. After the assembly, the inner radius of the inner cylinder is equal to a, the contact radius is equal to b and the outer radius of the outer cylinder is equal to c.

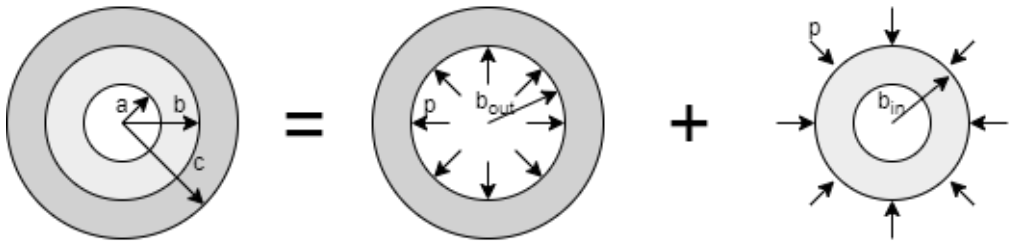

Figure 3.12: *Interference contact pressure question can be solved as a superposition of two thick-walled cylinders with pressure equal to contact pressure acting on outer and inner surface of respectively inner and outer cylinder.*

The contact pressure acting on the inner surface of the outer cylinder and outer surface of the inner cylinder results in the radial deformation of these surfaces denoted respectively $u_{\text{out},r=b}$ and $u_{\text{in},r=b}$. The radial deformations must satisfy Equation 3.1 [29], where δ is the radial interference between the cylinders.

$$u_{\text{out},r=b} - u_{\text{in},r=b} = \delta \tag{3.1}$$

The radial displacement of the thick-walled cylinder (elastic modulus E, Poisson number ν) with the inner radius r_{in} and outer radius r_{out} acting under inner pressure p_{in} and outer pressure p_{out} are described with following equations [2]:

$$u_{r=r_{\text{in}}} = \frac{p_{\text{in}} r_{\text{in}}}{E}\left(\frac{r_{\text{out}}^2 + r_{\text{in}}^2}{r_{\text{out}}^2 - r_{\text{in}}^2} + \nu\right) - \frac{p_{\text{out}} r_{\text{in}}}{E}\frac{2r_{\text{out}}^2}{r_{\text{out}}^2 - r_{\text{in}}^2} \tag{3.2a}$$

$$u_{r=r_{\text{in}}} = \frac{p_{\text{out}} r_{\text{out}}}{E}\frac{2r_{\text{in}}^2}{r_{\text{out}}^2 - r_{\text{in}}^2} - \frac{p_{\text{out}} r_{\text{out}}}{E}\left(\frac{r_{\text{out}}^2 + r_{\text{in}}^2}{r_{\text{out}}^2 - r_{\text{in}}^2} - \nu\right) \tag{3.2b}$$

From the equations 3.3 the equations describing $u_{\text{out},r=b_{\text{out}}}$ and $u_{\text{in},r=b_{\text{in}}}$ can be derived.

$$u_{\text{out},r=b_{\text{out}}} = \frac{p b_{\text{out}}}{E_{\text{out}}}\left(\frac{c^2 + b_{\text{out}}^2}{c^2 - b_{\text{out}}^2} + \nu_{\text{out}}\right) \tag{3.3a}$$

$$u_{\text{in},r=b_{\text{in}}} = -\frac{p b_{\text{in}}}{E_{\text{in}}}\left(\frac{b_{\text{in}}^2 + a^2}{b_{\text{in}}^2 - a^2} - \nu_{\text{in}}\right) \tag{3.3b}$$

Inserting the formulas for $u_{\text{out},r=b_{\text{out}}}$ and $u_{\text{in},r=b_{\text{in}}}$ into the equation 3.1, the formula for p can be obtained (Equation 3.4). It can be further simplify by approximating b_{in} and b_{out} as b.

$$p = \frac{\delta}{b\left(\frac{1}{E_{\text{in}}}\left(\frac{b^2+a^2}{b^2-a^2} - \nu_{\text{in}}\right) + \frac{1}{E_{\text{out}}}\left(\frac{c^2+b^2}{c^2-b^2} + \nu_{\text{out}}\right)\right)} \tag{3.4}$$

The stress distribution in the cylinders along the radius r can be then easily calculated from the formulas describing tangential stress σ_t and radial stress σ_r of a thick-walled cylinder with a pressure p acting on respectively outer and inner surface [2].

- For the inner cylinder:

$$\sigma_t = -\frac{pb^2}{b^2 - a^2}\left(1 + \frac{a^2}{r^2}\right) \quad \sigma_r = -\frac{pb^2}{b^2 - a^2}\left(1 - \frac{a^2}{r^2}\right) \tag{3.5}$$

- For the outer cylinder:

$$\sigma_t = \frac{pc^2}{c^2 - b^2}\left(1 + \frac{b^2}{r^2}\right) \quad \sigma_r = \frac{pc^2}{c^2 - b^2}\left(1 - \frac{b^2}{r^2}\right) \tag{3.6}$$

However, the presented calculation method cannot be used in the case the outer cylinder is replaced with a split ring. Not being able to consider the case axisymmetrical, greatly adds to the complexity of the task as the pressure distribution and displacements become unevenly distributed along the split ring. The analytical solution to this problem is not known, so to perform the calculations for such a case, one must approximate the problem to a thick walled cylinders problem.

The stress and pressure calculations for a split ring have been attempted previously, but they tend to be situation-specific. E. Dragoni and A. Stronzi describe in their paper, a split ring being inserted into a circular housing [5]. The findings from this paper helped us verify the behavior of our model, but the theories used in that paper cannot be applied to our case and the approximations made cannot be used for the case presented in this project. If the same equations and assumptions are considered the values of torque and pressure are different from what is seen experimentally. So these theoretical methods can be used to verify the behavior of the model, i.e they can be used to check the behaviour of the contact pressure. This check can tell us if the simulated model is behaving close to real life condition. But they are not a reliable hand calculation model, as the values they predict have too high an error.

4 Methods

This chapter will cover the overview of the methods that were used during the study. It will focus on the Finite Element Method, Finite Element Analysis, and the experiment design. Besides the theoretical aspects of each topic, case-specific details regarding the friction hinge analysis will be described.

4.1 Finite Element Method

The Finite Element Method (FEM) is widely used in engineering for numerically solving partial differential equations. Its applications range throughout nearly all engineering disciplines and include such examples as solving heat distribution problems, performing fluid mechanics simulations, and evaluating the strength and performance of various components such as bridges, machine elements, or biomedical prostheses. [33] The practical use of FEM as an engineering tool is called Finite Element Analysis and will be described in more detail in the next section.

FEM in principle divides a complex problem into several small ones. To do so, the geometry is discretized into finite elements, where for each element the solution to the partial differential equations is approximated [33]. The displacements and stresses are calculated from the equilibrium conditions for the whole structure. That way a complex geometry and boundary conditions problem can be broken down simplified and solved relatively easily compared with finding the analytical solution for the initial problem, which often does not even exist.

The formulation of the Finite Element Method will not be explained here in detail. For information regarding Finite Element Method formulation please refer to such literature as Zienkiewicz [36], Kurowski [21] and Singiresu [33].

4.2 Finite Element Analysis

The Finite Element Method is only a theoretical foundation to numerically solve partial differential equations. Its practical use is called Finite Element Analysis. By using FEA, the costly and time-consuming prototyping and physical testing can be to large extent replaced by virtual analysis. This is not only more cost and time-effective, but by aiding the design decision with FEA it is possible to perform significantly more design-simulate iterations and thus create stronger, more lightweight, and better-performing components than it would be attainable using the design-prototype-test approach [21]. To perform FEA several open-source and commercial software are available, such as Matlab, Code Aster, Octave, ANSYS, COMSOL Multiphysics, Abaqus, etc. In this study, ANSYS Workbench 2021 R1 was used.

FEA involves several additional activities both as a preparation for FEM and post-processing. The procedure can be divided into four following steps:

1. **Pre-processing** This step involves activities such as geometry and mesh preparation, material assignment, loads and boundary condition definition, and contact definition. The goal here is to simplify the physical geometry and loads into their digital representation in a format appropriate for FEM. This step drives the quality of the whole simulation and must be performed with care and attention. Often to find a good combination of mesh, loads, and boundary conditions several iterations must be done.

2. **FEM** With the input from the pre-processing step, the primary (displacements) and secondary unknowns (stress and strain) are calculated.

3. **Post-processing and visualization** The results from the FEM need to be presented in an easy to interpret form. These can include plotting the distribution of the unknown, making graphs of the maximum and minimum values, and calculating the moment reaction.

4. **Engineering judgment** The visualized results must then be assessed regarding their quality. If it is decided that the simulation is sufficiently accurate, the conclusions can be drawn from it. If the results are nonphysical, the whole process must be re-iterated starting with step 1.

As mentioned, the pre-processing step is crucial to perform a good simulation and will be described further in the next section. The section will also include case-specific details.

4.2.1 Pre-processing

The preparation for the Finite Element Method requires in-depth knowledge about the loading conditions of the component, its geometry, and material, as well as being familiar with the FEM theory and the used FE software. How the pre-processing is done will be a driving factor not only for the quality of the simulation but also for the computing time. The number and degree of the equations approximating the partial differential equations will influence how long will it take the simulation to find a solution to the problem. Usually the more elements and the higher their order, the longer the computing time will be. Similarly, the non-linear boundary conditions and contact formulation are often more accurate, but they increase the solution time. Therefore it is important to find a balance between the degree of approximation and the time it takes to solve.

Geometry

To prepare geometrical input for FEM, the digital representation of the component must be produced. This can be done either in 3D or the geometry can be simplified into 1D or 2D. Even in 3D simulations, the geometry is often geometry-optimized by simplifying non-load carrying elements, especially when the geometry is complex and the number of finite elements required to map them is significant [21].

To simplify the friction hinge geometry, the Left, Right and Middle part of the hinge assembly were replaced by boundary conditions . By doing so the need for a geometrical representation of the spline connections on the shaft ends was removed and the number of elements required to mesh the component decreased considerably. Some features such as chamfers and edge blends had to be removed as well. By performing these operations it was possible to reduce the simulation time from a couple of hours to minutes while maintaining a good degree of approximation. the simplification of geometry is shown in Figure 4.1.

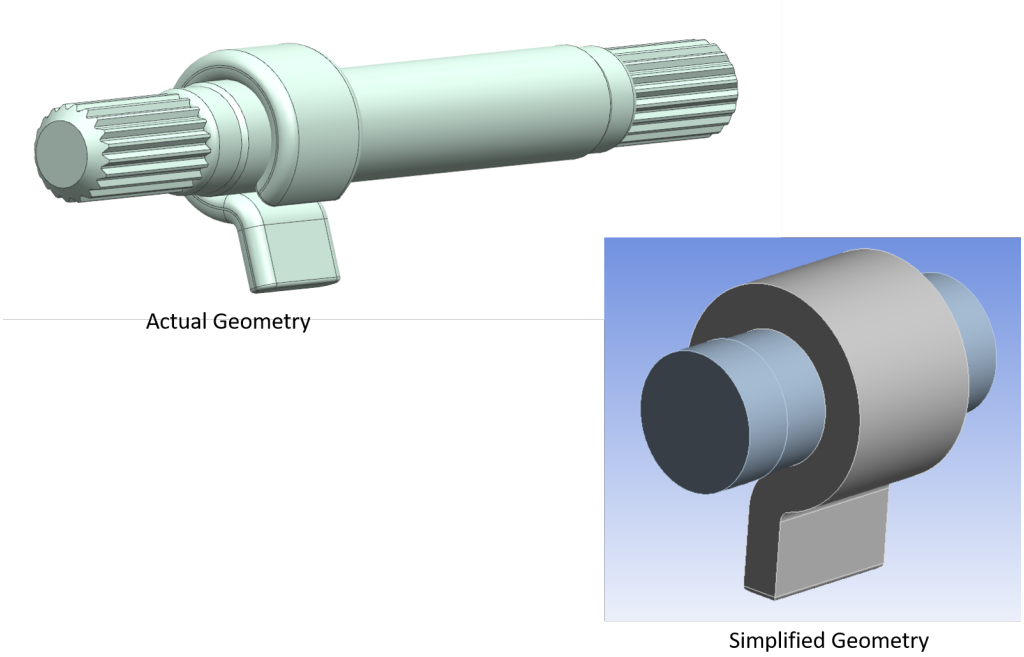

Figure 4.1: *Simplification of the geometry.*

A 2D representation of the hinge was also created to test whether the results of the model would be comparable with the 3D simulation. 2D models are significantly less computationally demanding, therefore a larger number of iterations of the simulation set-up could be performed in the same time when compared to a 3D simulations .

2D simplification of a 3D model is usually done by assuming one of the following states: plane stress, plane strain, and axisymmetric (Figure 4.2) [36, 21]. Plane stress assumption is applicable for components where the third dimension is much smaller than the other two, here it can be approximated that the only non-zero components of stress are the ones in the plane of the problem. For the bodies where the third dimension is much larger, a plane strain assumption can be made. In this case, all the strain components in the normal

direction of the surface are considered equal to zero. Finally, in the axisymmetric bodies in the cylindrical coordinate system $r - \theta - z$, displacement, stress, and strain values are assumed to be independent of θ.

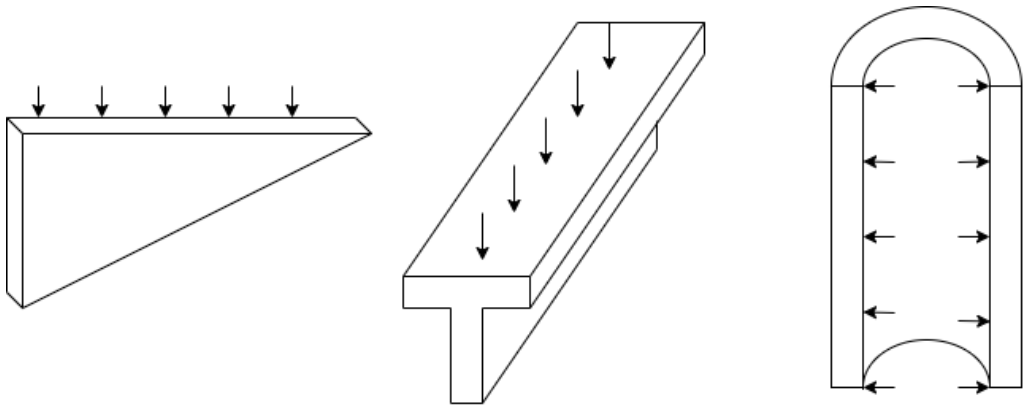

Figure 4.2: *Examples of three-dimensional bodies that can be approximated with the two-dimensional models. Left: plane stress, middle: plane strain, right: axisymmetric.*

For the friction hinge, both the plane strain and plane stress model are tested. In ANSYS, the plane stress model can be assigned a thickness and it shows a behavior close to the 3D simulation. The plane strain option in ANSYS does not allow the 2D surface to have a thickness and hence produces results that cannot directly be compared to the results seen in 3D. To overcome this a generalized plane strain setting can be used which would consider a plane strain assumption with thickness. This produces similar values as the plane stress assumption. Considering the scale of the model it does not fit into either of the assumptions, however, the expected results when compared to a 3D model suggest that both models can give good results. Since both the assumptions predict the stress and contact pressure similarly, we use the plane stress assumption for all further 2D analysis.

It is important to note that the model does not fulfill the requirements for the plane stress or the plane strain completely, since the thickness of the part of the shaft is not significantly bigger than its diameter nor is the diameter significantly bigger than its thickness. The viability of the approximations is tested by comparing them to the 3D model. The comparison between the two is made in the Section 5.1.3

Material models

The materials used for the production of the shaft and part on the shaft were respectively High-Speed Steel (HSS) and Stainless Steel 316L. Since the shaft should only experience stresses in the elastic range, the stress-strain behavior model of the HSS can be linear elastic. In the case of the part on the shaft, some areas of the component reached the yield limit and plastic deformations occur. In this case, the linear elastic model would overestimate the stress values. Therefore, a bi-linear hardening model is chosen.

The material properties are considered as per GRANATA EDUPACK 2020. They are listed in the Table 4.1. The last row contains graphs that give the overview of the stress-strain relationship models; these graphs do not represent real values, but rather the general shape of the curves.

Boundary conditions

In the Finite Element Analysis, the two most common types of boundary conditions are essential (also called Dirichlet) and natural (also called Neumann). The essential boundary conditions are imposed on the primary variables (e.g. displacement). They are enough to solve the partial differential equations. Natural boundary conditions involve derivatives of the primary variables (e.g. forces and moments). They are automatically satisfied by the FEM equations and they are not enough to solve them - at least one essential boundary condition is needed. In the Finite Element Analyses done during the study only essential boundary conditions were used, hence the main focus will be placed on them.

The essential boundary conditions are applied to the degrees of freedom of the element by either fixing it in place, forcing a change of some fixed value, or leaving it free to move. In the three-dimensional solid elements

Parameter	Part on shaft	Shaft
Material	Stainless steel 316L	High speed steel (HSS)
Young's Modulus	2e+05 MPa	2,2e+05 MPa
Poisson's Ratio	0.3	0.3
Compressive Yield Strength	250 MPa	230 MPa
Tensile Yield Strength	250 MPa	230 MPa
Tangent Modulus	1330 MPa	-
Stress-strain model	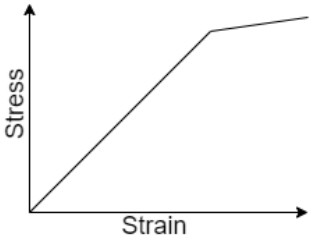	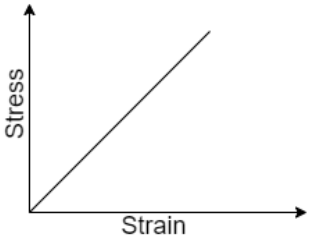

Table 4.1: Material properties.

each node has three degrees of freedom per node, while in the two-dimensional plane strain case, each node has only two degrees of freedom per node.

In the study, three types of boundary conditions were used: fixed support, frictionless support, and remote displacement. Fixed support is a boundary condition that prevents movement and deformation in all degrees of freedom. It is often used to anchor the component in one place and prevent rigid body movements. The frictionless support prevents any movements and deformations in the direction normal to the face, leaving the surface free to deform in the tangential direction. The remote displacement is used to apply the displacements and rotations at an arbitrary remote point [27]. This boundary condition is can be used to rotate a component around a point or axis, e.g. the shaft, as it was done in the friction hinge case.

Contact definition

When more than one body is involved in the analysis, contact modeling is introduced to take into account how the components interact with each other. Depending on the contact definition, the bodies in contact may penetrate each others boundaries to some extent, but to keep the model realistic, this value should be minimal. Through contact normal compressive forces and tangential friction forces can be transferred [27].

An important aspect of defining contacts in the friction hinge model was the interference fit between the parts on the shaft and shaft. Interference could be modeled either by creating a CAD model of the parts that would already include it or by using the *geometrical modification* feature in ANSYS Mechanical contact definition. In the first method (Figure 4.3a) the geometry needs to be modified every time an iteration needs to be simulated. Furthermore, the interference load is always applied instantly, which often creates convergence issues as the penetration force is exaggerated.

The second method would allow defining the interference fit by adding the virtual offset to one of the contact surfaces without actually editing the geometry of the components. This procedure, illustrated in Figure 4.3b, could be done either with *Add offset* or *Offset only* option. The first one directly adds the offset to the geometries, while the latter first close all the initial gaps and penetrations. Since the geometry of the hinge did not have any initial interference, the first option was chosen. The loading resulted from the applied offset could be ramped, where it was gradually applied during the first second, or be applied immediately.

For the contact between the shaft and the part on the shaft the second method was used with the following setting: *Add Offset, Ramped Effects.*

Meshing

In FEM it is not the CAD geometry that is the basis for the calculations, but the mesh [21]. It is therefore only natural that the mesh plays an important role in the quality of results that are obtained from the calculations. As mentioned, a proper balance between the type of mesh and the solving time needs to be found.

In general, the deformations, and hence the stress and strain values, are underestimated in FEM. This error is reduced and the result converges to the real solution as the mesh is improved, e.g. by reducing the size of

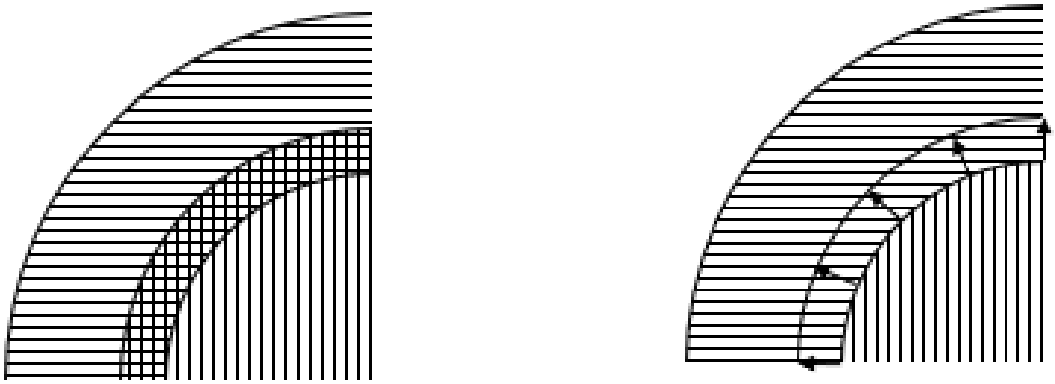

(a) *A schematic representation of Geometrical offset. No additional changes in the calculations are required.*

(b) *A schematic representation of Add Offset setting. Geometrically, the two bodies do not intersect, but during the calculations, virtual offset is taken into consideration.*

Figure 4.3: *Two ways of creating the intersection fit between the shaft and part of shaft.*

the finite elements or increasing the order of elements [21], [33].

Mesh refinement can be either done across the whole body or just in selected areas. It is common to refine the mesh in the "most interesting parts" of the component, i.e close to the boundary conditions and in the areas with high stress or large deformations [33]. The polynomial order of the shape function is usually set to either linear or quadratic. The difference between the former and the latter is that in quadratic elements, the nodes are placed not only in the corners of the element but also in the middle of each edge [21]. The mesh can be altered as well by changing the element type, e.g. triangular or quadrilateral in 2D and tetrahedrons or hexahedral in 3D.

Large displacement

One of the analysis settings in ANSYS Mechanical is *Large Deformation on/off*. With *Large Deformation on* a non-linear geometry model is assumed, meaning the stiffness matrix is also influenced by the changes to the geometry during deformation and is recalculated every couple of iterations. This setting is advisable to use when the displacements exceed 5% [21] of the characteristic model dimension. As in any other non-linear simulation, computational time increased. However, in linear analysis due to the high deflection results in a "swelling" of the component in the case of shafts - each element travels along the direction normal to the shaft radius, so the shaft diameter appears to increase.

4.3 Experimental study

To validate the FEA model test values are required. However, the ones provided by IKEA and INDAUX, described in proved to be inconsistent and their quality had to be reassessed. Therefore a new experiment was planned, taking into account all the learning's from the previous experiments not to repeat the same mistakes and errors as the previous attempt and obtain high-quality results.

4.3.1 Measurement method

One of the tasks to be completed during this project was to review the torque measuring method and identify if there is a more reliable way to perform the testing.

As mentioned in , the currently used method is not very precise and heavily depends on the skills of the person performing the experiment. There existed a need for a more robust technique that would utilize only the basic equipment. The measuring set-up proposed is presented in Figure 4.4. Similar to the previous method, the shaft is held in place using a vice and the shaft is the moving component. The shaft is connected to the arm in the middle of it. The reason for that is for the weight of the arm not to induce any additional torque on the shaft. The measurements of the torque are performed using the force measuring dynamometer attached to the

arm by the holes placed in known distances from the shaft center. Depending on which hole the dynamometer is attached to, different ranges of the tool can be used - and hence different accuracies can be obtained.

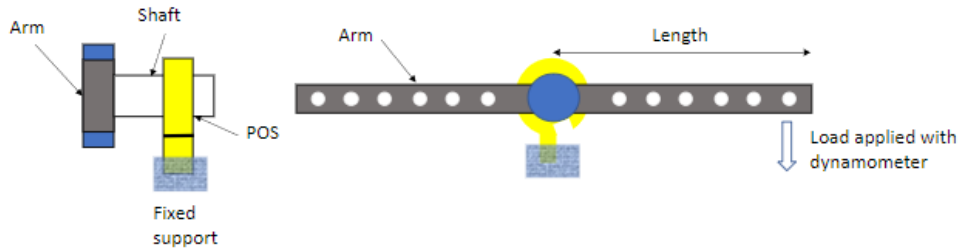

Figure 4.4: *The schematics of the torque measuring method. The force needed to initiate movement of the shaft is measured using dynamometer attached to the arm on a known distance from the shaft center.*

This method has been tested before proposing it to INDAUX to validate its robustness. For that, a simple setup comprised of a 3D-printed shaft and arms, a water bottle as the load, and a dynamometer were used (Figure 4.5).

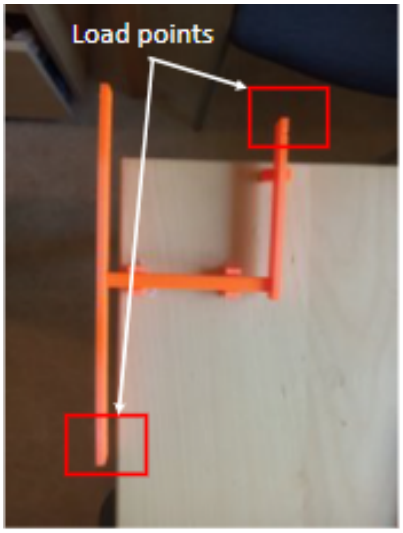

(a) *The view from above on the testing. The water bottle with known weight was attached an one end of the shaft and dynamometer - on the other.*

(b) *Front view of the testing. Both the dynamometer and the load (water bottle) can be observed.*

Figure 4.5: *The overview on the testing of the torque measuring method.*

During testing, it was evident that the plastic shaft deforms under the torsional load. Therefore there is about a 12-17% difference between the torque applied and torque measured (Table 4.2). However, the measurements were consistent, meaning that during repetitive measurements for each load the value read on the dynamometer was roughly the same. This was considered sufficient to prove the robustness of the method.

Torque applied	**Torque measured**	**error**
0.283 Nm	0.234 Nm	17%
0.372 Nm	0.327 Nm	12%

Table 4.2: The results of the testing of the torque measuring method.

Scenario no	Diametrical interference	Inner diameter of part on shaft (POS)	Thickness of POS	Diameter of shaft	Assembly position of POS	Number of samples requested
1	INT A	ID A	THK A	OD A	LLLR	3
2	INT A	ID A	THK B	OD A	LLLR	3
3	INT A	ID A	THK C	OD A	LLRR	2
4	INT A	ID A	THK C	OD A	LRLR	2
5	INT A	ID A	THK D	OD A	LRLR	3
6	INT A	ID B	THK A	OD B	LRLR	3
7	INT A	ID C	THK A	OD C	LRLR	3
8	INT A	ID D	THK A	OD D	LRLR	1
					Total:	**20**

Table 4.3: The specifications of prototypes ordered.

4.3.2 Prototype samples ordered

Once the measuring method has been established, the prototypes had to be ordered. The project's budget allowed for manufacturing around 20 samples. This gave the opportunity to either have many samples with different dimensions to closely study the various parameters' influence on torque value or to manufacture many prototypes of the same dimensions to obtain results whose quality could be easily assessed.

The decision was made to follow a mix of both approaches. Three parameters were chosen for the influence study - diameter of the shaft, the thickness of the part on the shaft, and assembly position of the parts on the shaft. The two first parameters were checked separately with at least 3 samples for each specification produced to account for variations of manufacturing. Assembly position influence on the torque generated by the hinge was checked alongside previous parameters.

All specifications for requested samples can be found in Table 4.3. The columns *Diametrical interference* and *Inner diameter of part on shaft* are there only for information purposes since they do not contain tested parameters. The interference was kept constant and the ID of POS is a result of calculating *Shaft diameter - diametrical interference*.

The L and R symbols in *Assembly position* column denote different ways of assembling the POS, as the POS induces different torque in the clockwise and anticlockwise direction. Assuming the first POS have the gap on the left side of the flange, the rest of the POS should be assembled either with the gap on the same side (L) or on the opposite - right - side (R) according to the *Assembly position* column.

5 Finite Element Model

The objectives of establishing the FEM model are to calculate the stresses in the parts and estimate the torque required to overcome the friction produced by the interference fit.

To create this FEM model, ANSYS Workbench software is used. The geometry is modeled/modified with SpaceClaim and DesignModeler, both modules are available in ANSYS Workbench.

5.1 Pre-study simulations

This section documents the various iterations conducted during this project. It aims to give the reader an idea of the development process for the FEM model.

The source geometry for the friction hinge is a 3D CAD file. While 3D models tend to be the most accurate compared with 2D or 1D approximations, they are also computationally expensive. Thus to verify the behavior of the model, all analyses are set up in 2D first. Once the behavior is verified, a 3D model with similar boundary conditions is set up. Table 5.1 outlines the simulations carried out to establish the model and boundary conditions.

The points of interest are to check the stress distribution, deformation, contact pressure, and moment reaction against the rotation of the shaft. The stress distribution will allow verifying if the model is behaving as expected and whether the POS is strong enough for the hinge operation. Similarly, the total deformation will help verify the model and provide insight into the hinge operation. Additionally, deformation visualized at an enlarged scale helps to verify the forces acting in the system and brings to light any erroneous deformations.

Test no	Test name	Objective
1	Cylinders in interference	1D axisymmetric model of interference fit
2	2D simulation of the friction hinge	Test boundary conditions and results
3	3D simulation of the friction hinge	Test boundary conditions and results
4	2D simulation of hinge with the Stop	Improve model behaviour
5	3D simulation of hinge with the Stop	Improve model behaviour

Table 5.1: Description of tests.

5.1.1 Cylinders in interference

To understand the ANSYS environment better, geometry is created in SpaceClaim to simulate two cylinders assembled with an interference fit. This is the geometry for which a hand calculation model is available (as discussed in the section 3.3), so it is easy to validate the model. This analysis is carried out in 2D. Both the shaft and the sleeve are assumed to be made of structural steel, a standard material available in ANSYS.

Geometry and Boundary conditions

Two cylinders with intersecting geometries are created in SpaceClaim. For this analysis, the initial geometry considered is described in Table 5.2.

Part	**Dimension**	**Value**
Shaft	Diameter	OD E
Sleeve	Inner diameter	ID A
Sleeve	Outer Diameter	ID A + 2*THK A

Table 5.2: Dimensions of cylinders.

The geometry and the mesh are shown in Figure 5.1a. To keep the number of elements low, quad elements are used. The boundary conditions for this analysis are kept very simple. The position of the shaft is determined by remote displacement B and the sleeve - by remote displacement A, as shown in Figure 5.1b. The simulation

is carried out with 5 load steps. The first step allows the geometries to normalize the interference. The following load steps gradually induce a rotation to the shaft to 5°. Dividing the rotation into several steps means that each step has smaller displacement and force values which help with solution convergence. Figure 5.2 presents a schematic of the rotation introduced to the shaft through the remote displacement.

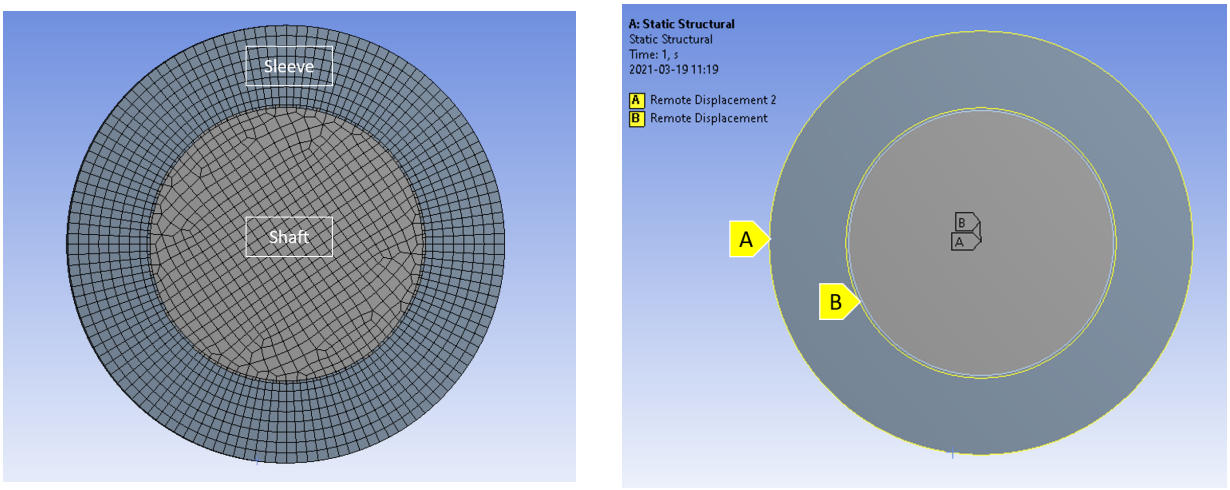

(a) *Geometry and mesh of cylinders.*

(b) *Boundary condition*

Figure 5.1: *Basic Setup for FEM analysis of cylinders.*

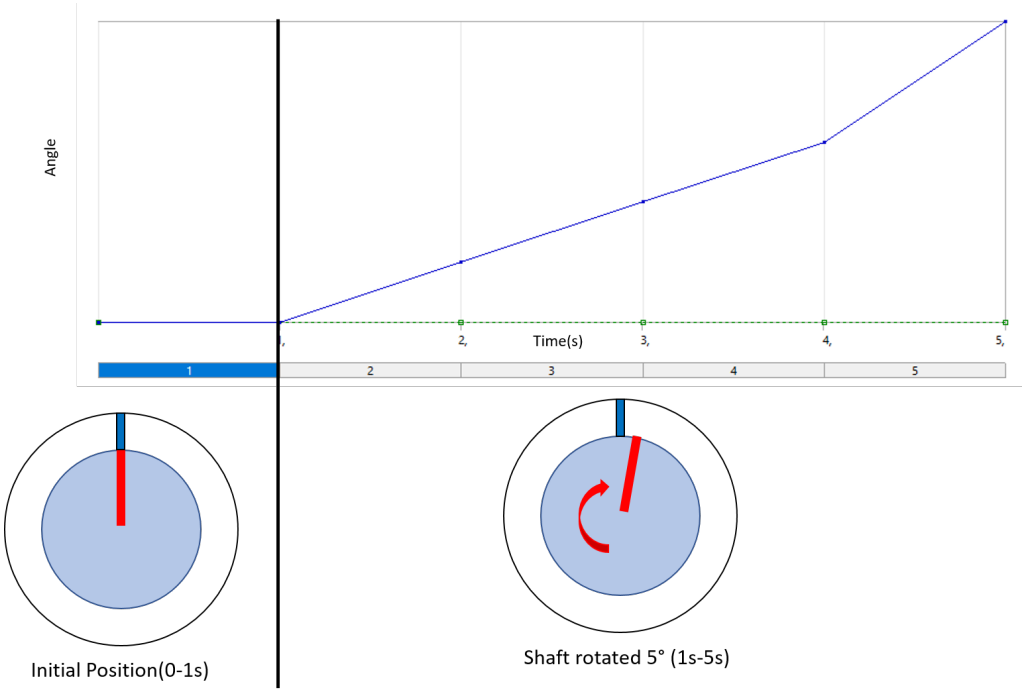

Figure 5.2: *Schematic of the remote displacement.*

Contact

This system has two surfaces in contact: the outer circumference of the shaft and the inner circumference of the sleeve. A frictional contact with a coefficient of friction of 0.1 is assumed for this simulation. The interference is introduced as a ramped geometric offset as this approach helps the FE model converge better when compared with introducing intersecting geometries. Both methods of introducing interference can be interchanged without

affecting results. For this simulation intersecting geometries are used.

Results

The results of the comparison between the FEM simulation and the theoretical calculation for the same geometry can be seen in Figure 5.3. The stress distribution is uniform and axisymmetric. The contact pressure is also more or less uniform with some irregularities seen due to approximation of the geometry using a Finite element mesh.

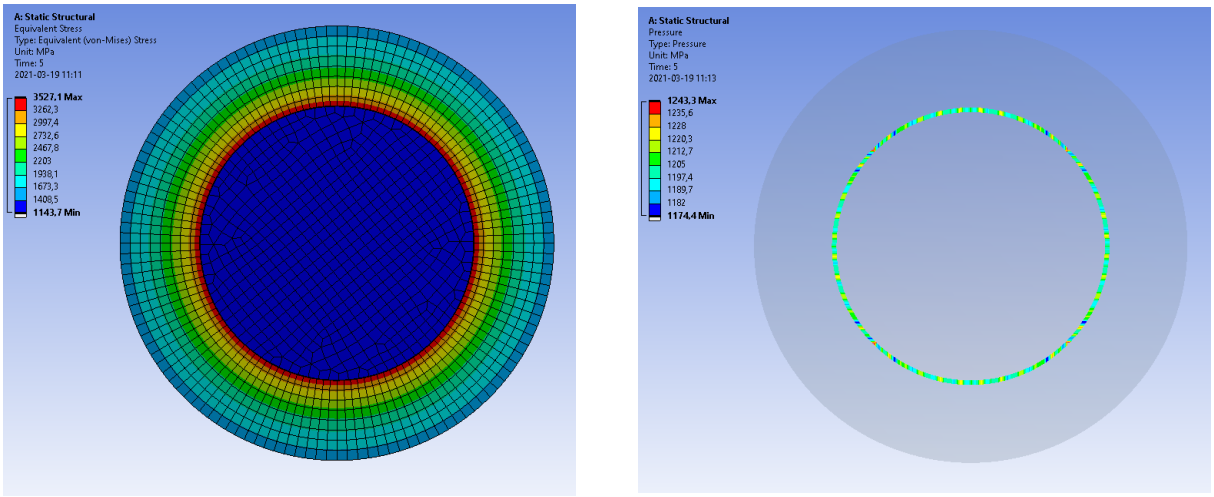

(a) *Equivalent stress distribution in the cylinders.* (b) *Contact pressure between the cylinders.*

Figure 5.3: *Cylinders Simulations results.*

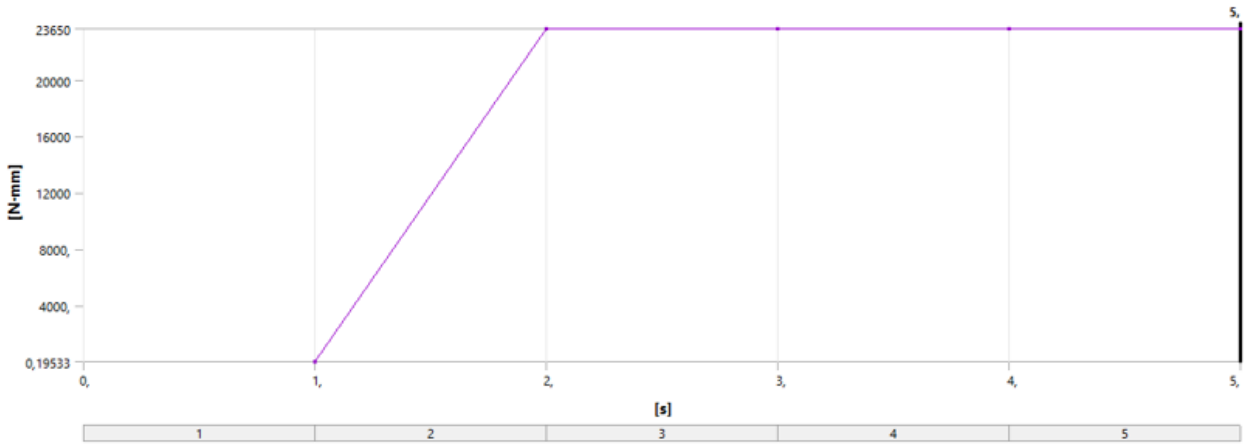

Figure 5.4: *Torque plot.*

It is important to note that even for a low interference of 0.1 mm the sleeve has maximum stress of 3527 MPa, which is considerably higher than the yield strength of the material. It indicates that using a perfectly elastic material model would not be accurate. If the perfectly elastic material model is considered, the part would have been damaged as the stress seen in the component much higher than the yield strenght of the material. The material is not operating in the perfectly plastic range, thus a bi-linear model might be used in the later models of the hinge if the stress levels are also considered in that case. However, since the hand-calculation model assumes a perfectly elastic material as well, it is correct to use this material model for the sake of comparison.

Figure 5.4 shows the torque plot for the analysis. At step 2 rotation is applied to the shaft as it is clearly seen on the graph: the moment reaction on this boundary condition ramps to a particular value and remains constant throughout the rotation. This is expected since the contact model does not take into account the difference between the coefficient of static and dynamic friction (which is slightly lower than static friction).

Table 5.3 shows the comparison between the FEM simulation and the analytical solution for the 1D axisymmetric model. The differences in torque between these models are very small. Thus it can be concluded that a well-calibrated model can be used to get results whose accuracy can be trusted.

Output	**Axisymmetric model**	**FEM Result**	**Variation from axisymmetric calculation**
Contact pressure	1168.7 MPa	1204.5 MPa	3%
Torque	22.44 Nm	23.65 Nm	5.4%

Table 5.3: Theoretical calculations for 1D axisymmetric model vs FEM results.

5.1.2 2D simulation

Based on the observations from the cylinder analysis. A 2D simulation for the hinge setup is created. For simplicity, a single part of the shaft is modeled on a shaft.

Geometry and Boundary conditions

The shaft is modeled as a simple circular surface and POS as a cross-section of the actual part. Their dimensions are shown in Figure 5.5a. The width of the components is not modeled but is set directly in the solver. It must be noted that the shaft and the POS do not intersect geometrically, but rather the interference is added with the geometry offset command.

The materials used for these simulations are the same as the materials used for prototyping the IKEA samples. And as per the observations from Section 5.1.1, a bi-linear hardening model is used to improve the accuracy of the model. The part on the shaft is assigned stainless steel 316L, and the shaft is assigned high-speed steel. The material details are listed in the table 4.1 in section 4.2.1.

The boundary conditions for this analysis are shown in Figure 5.5b and are as follows: the shaft is controlled by a remote displacement which restricts motion along the X and Y axis, and forces rotation of the body about the Z-axis. The part on the shaft is constrained with a displacement A, which prevents all motion along the X-axis but permits motion along Y. These conditions represent the operating conditions of the hinge.

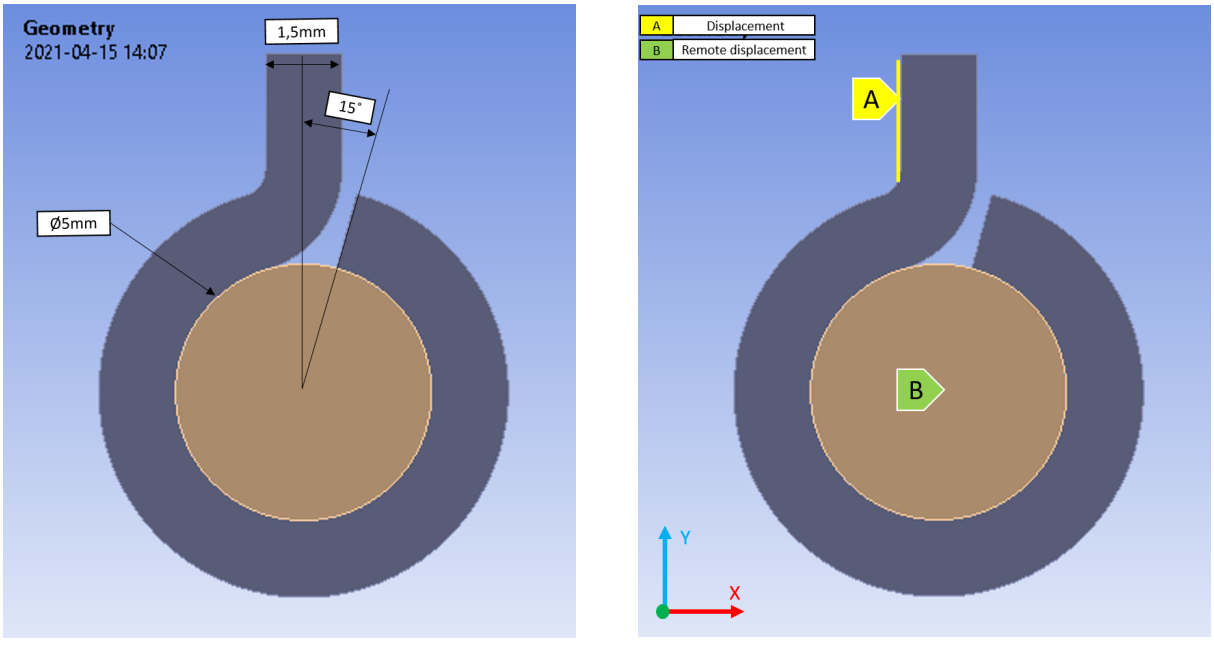

(a) *2D geometry.* (b) *Boundary conditions for the 2D analysis.*

Figure 5.5: *2D analysis.*

The setup of remote displacement B is shown in Figure 5.6. The first analysis is set up to check the rotation of the shaft in the counter-clockwise direction. The analysis is set up with 3 load steps, where in the first load step the shaft rotation was locked, in the next load step the shaft is rotated by 5°. During the last load step, the shaft is kept at 5°. Constraint A remains active throughout the analysis.

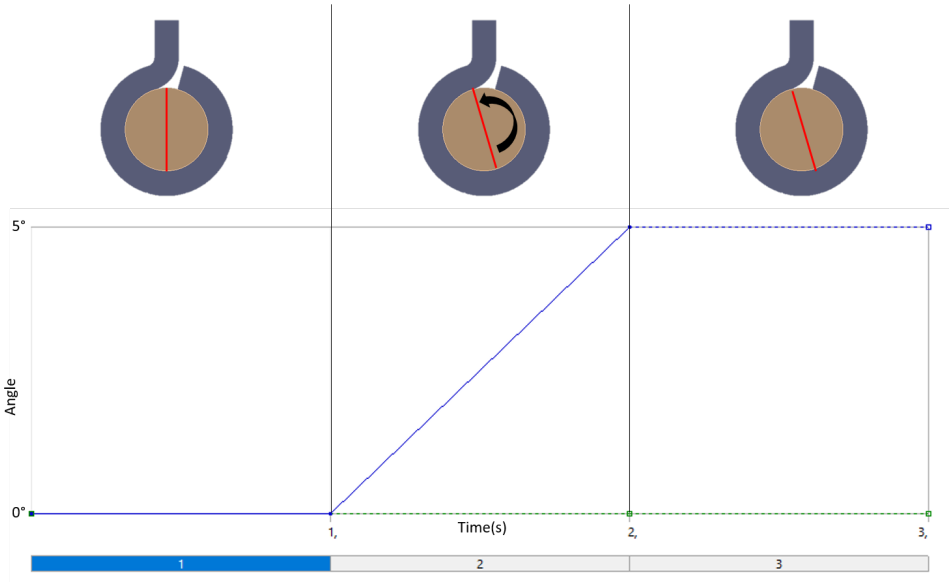

Figure 5.6: *Remote displacement setup for 2D analysis.*

In the second analysis with the same boundary conditions the rotation of the shaft was reversed and it rotated clockwise with the same load steps.

Contact

This analysis has one contact region, i.e between the shaft and the POS, which is assumed to be a frictional contact with the coefficient of friction as 0.1. This is the assumption used throughout most of the analysis since the frictional coefficient is a parameter for calibrating the FEM model. Pinball radius is a parameter used in contact formulation that allows the user to define contact search region [27]. The pinball radius for this contact region must be set to a value higher than the resulting interference. This is so that even after the offset the elements in contact should remain within the sphere of influence. If the pin ball radius is set at a value smaller than the offset, the target elements will no longer be considered in contact with the each other.

Mesh

The meshed geometry is shown in Figure 5.7. To generate this mesh both surfaces are assigned the Multizone method and a quad-dominant mesh is generated with a uniform surface mesh method and element size of 0,1 mm. Since this is a 2D analysis the elements are elongated along the thickness assigned to the geometry. This is a detail to keep in mind when going through the results. To verify the quality of the mesh, mesh metrics are used. If the metrics are close to reference values, the mesh can be considered as good. The reference values are Mesh Quality: 1, Aspect ratio: 1, Skewness (variation from the ideal shape of element): should not exceed 0.9, and the Jacobian ratio: close to +1.

5.1.3 Plane stress vs Plane strain

The 2D analysis is an approximation of the 3D dimensional model. As explained in Section 4.2.1, the approximation can be done in two ways: with the plane strain assumption where the $\epsilon_{zz} = 0$ and with the plane stress assumption where $\sigma_{zz} = 0$. In the 3D FEM model both the average stress in the Z direction and the strain in the Z direction were negligible, so it appears that for this particular model both these assumptions appear to hold good. Hence two simulations are run, one with each of the assumptions. However in the case of Plane strain, a generalised plane stress setting must be used, which can account for the width of the POS.

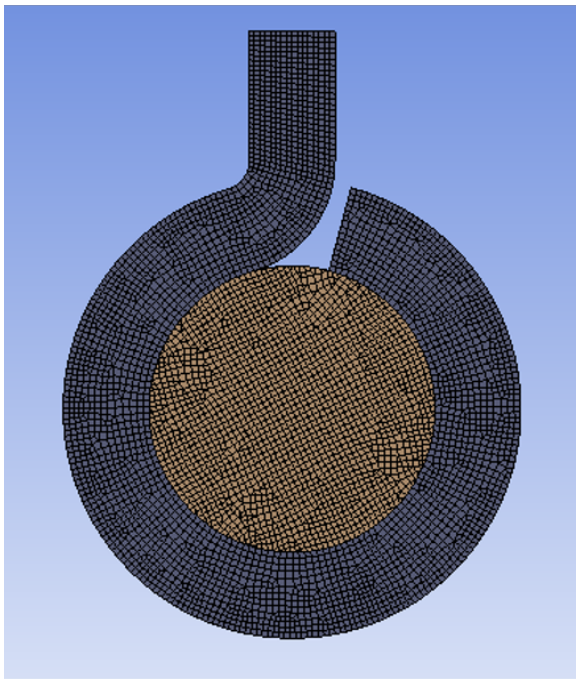

Figure 5.7: *2D analysis Mesh.*

It can be observed that the moment reaction in both the models is close to the 3D FEM model and since a standard plane stress model can be used it is preferred over the generalised plane strain model. Hence all the further 2D simulations are carried out with the plane stress assumption.

Results

The Von-Mises stress distribution is shown in Figure 5.8a. It clearly highlights the difference in stress-induced in a complete circle and a split ring. The split ring acts as a beam undergoing bending - the outer sections experience compression and the inner sections experience tension. A neutral axis between these two with low-stress levels is clearly visible. The complete ring, however, has a gradually decreasing stress in the radial direction throughout its section.

It can be noted that the deformation graph (Figure 5.8b) shows a slight gap between the two components. This is due to the geometric offset specified to simulate interference. This is also enhanced by visual scaling effects.

From the results of the simulation, it can be observed that as the interference is being normalized (load step 1) there is a torque acting on the shaft. This is probably because as the POS opens to account for the interference, due to the frictional contact, the POS exerts a rotational moment on the shaft. And at the end of this expansion, when the shaft starts to revolve by a certain value the torque is constant. It is also important to note that the torque required to rotate the shaft varies based on the direction of rotation. In general, the shaft needs greater torque to rotate in the direction that will close the gap of the POS and when rotating in the direction that would open up the POS, it needs a lower torque.

The figure 5.9 shows the moment reaction measured at the shaft. In the first time step, the shaft is held in place with 0° of rotation. A clear and steady rise in torque can be seen. This is the moment reaction due to the expanding POS. After the first load step, a rotation of 5° is applied to the shaft in the counterclockwise direction. It is seen that the torque steadily rises to about 427.84 Nmm. Figure 5.10 shows the torque values for when the shaft is rotated in the cloclwise direction. The torque plot rises when the POS is normalizing the interference, and then when the shaft begins rotation the torque value drops to the negative value and holds steady at -254.38 Nmm. This is the maximum torque offered by the POS in the negative rotation.

In the first second of the simulation, during the expansion, the torque rises almost to the operating torque value. It might at first look like an error, but it is the correct behaviour. Due to the fact that the bottom of the POS is fixed, the expansion of the POS results in similar situation as the rotation of the shaft. Hence the torque values for expansion and rotation are similar. If the POS wouldn't be clamped and instead it would be

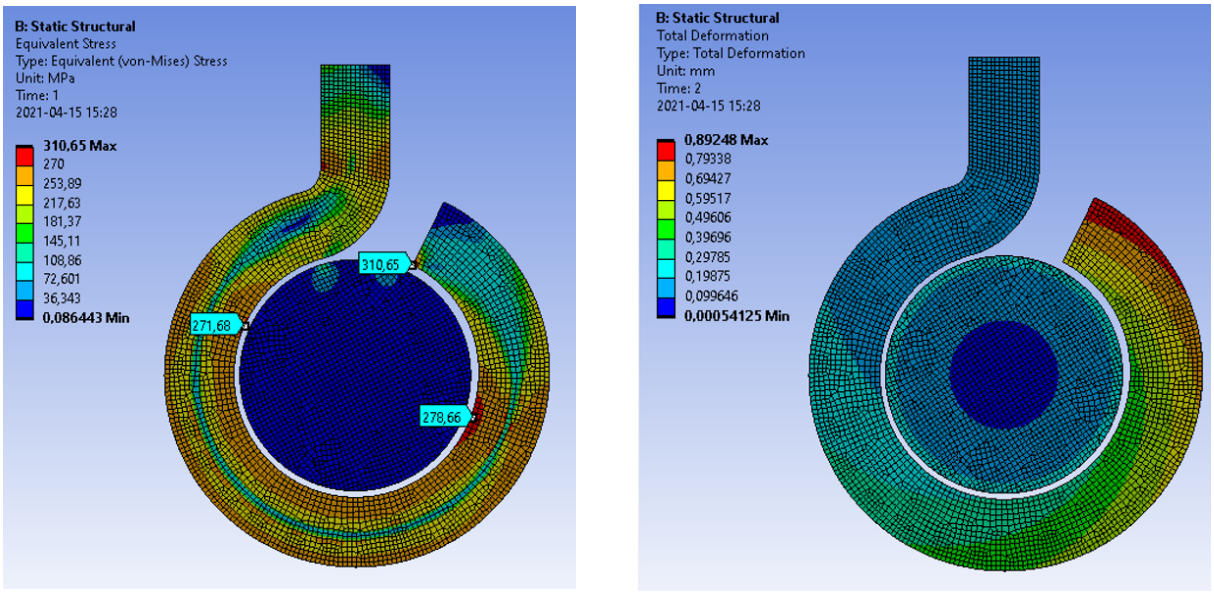

(a) *Von-Mises stress distribution in a 2D analysis.*

(b) *Total deformation in 2D analysis.*

Figure 5.8: *2D analysis results.*

free to move, the torque during the expansion would be 0 with the rotation torque being the same as in the model with a clamped POS. This is further discussed in section **??**.

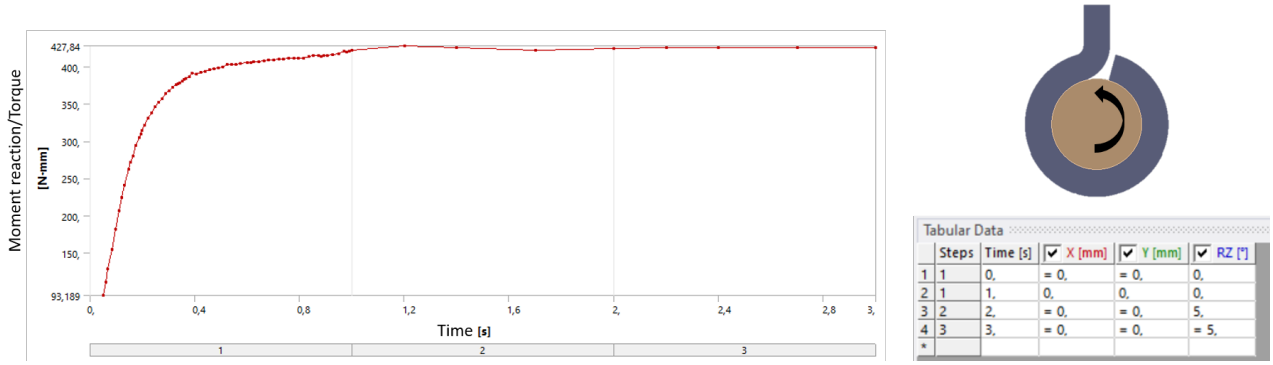

Figure 5.9: *2D analysis Torque values for counterclockwise rotation. The torque rises up to 1s due to the expansion of the POS and after the rotation starts it slightly increases further to the operating torque value.*

The pressure distribution of a split ring in interference is considerably different from that of a closed cylinder. Figure 5.11 shows the pressure distribution seen in the 2D analysis. The pressure is not evenly distributed across the circumference but is significantly higher at the opening of the split ring and around a region diametrically opposite to the opening on the ring. This is in line with the literature about split rings and has been recorded in patents and literature for this kind of setup [5] [23].

5.1.4 3D Analysis

After collecting observations and results of the 2D analysis, 3D model is built and analyzed to verify the 2D model. The geometry is the same as that used by IKEA.

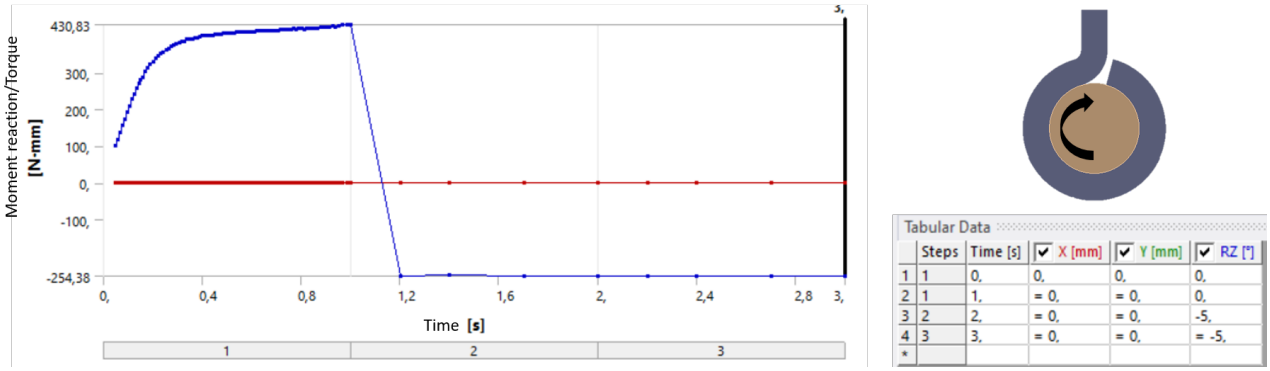

Figure 5.10: *2D analysis Torque values for clockwise rotation. The torque rises up to 1s due to the expansion of the POS and as soon as actual rotation starts it drops to the operating torque value.*

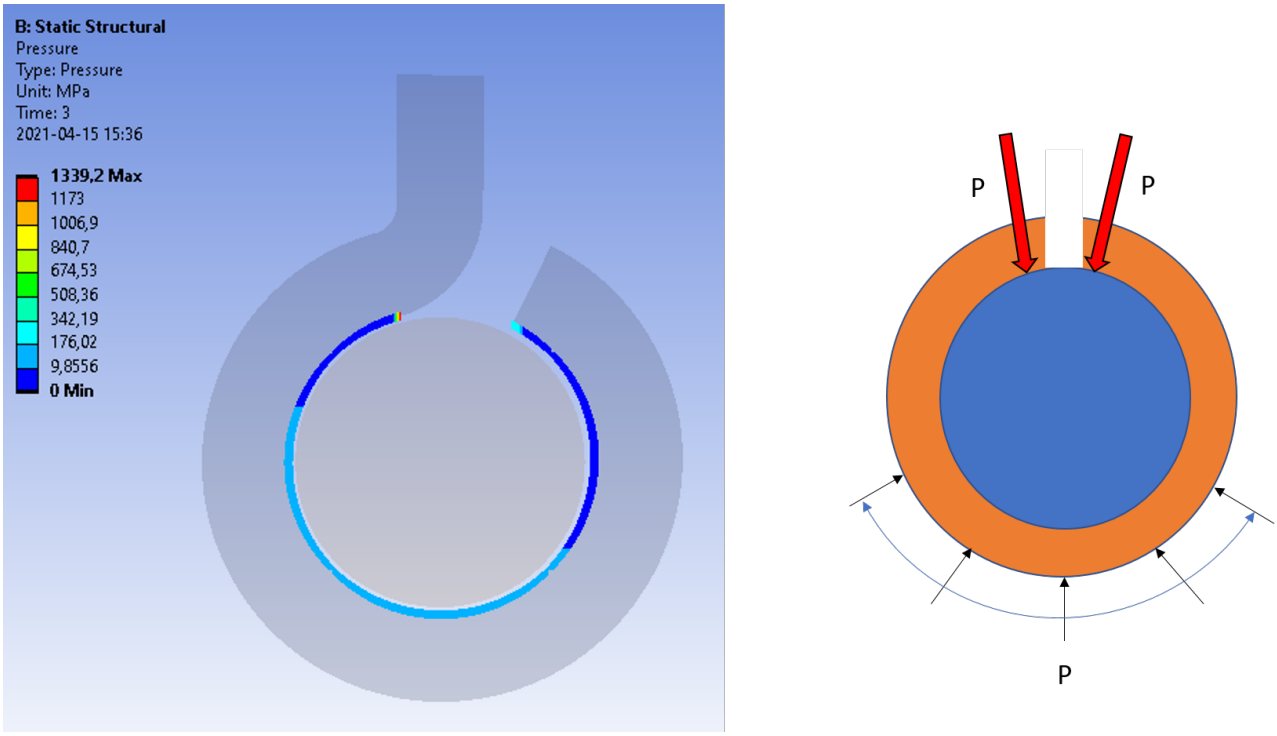

Figure 5.11: *2D analysis pressure distribution.*

Geometry and boundary conditions

The dimensions for the 3D geometry are the same as the 2D analysis (Figure 5.12a). The primary difference between the two analyses is that the 3D analysis has several elements across the thickness, whereas the 2D will only have a single one.

A greater number of boundary conditions are required for this analysis. The boundary conditions are described in Figure 5.12b. The frictionless support A is used to restrict the rotation of the POS by blocking the displacement of the selected area perpendicular to the surface. The frictionless support B is used to restrict the motion of the shaft along the Y-axis (along its axis). Similarly, the remote displacement C is used to restrict the motion of the POS in the Y-axis. The remote displacement D is used to control the rotation of the shaft. The rotation is locked at 0° for the first time step and rotates by 5° in the second time step.

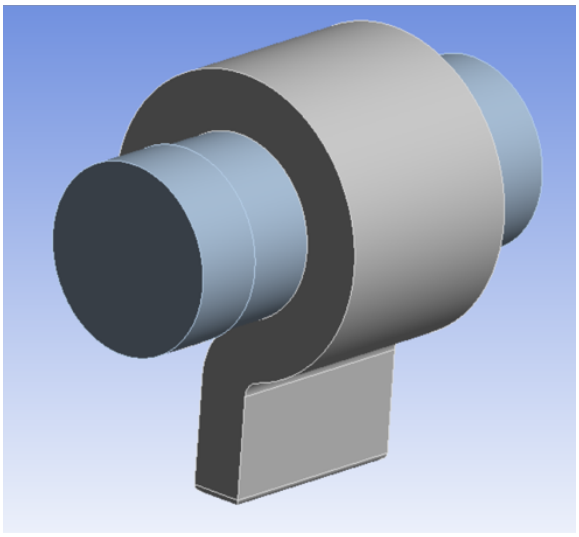

(a) *Geometry for 3D analysis.*

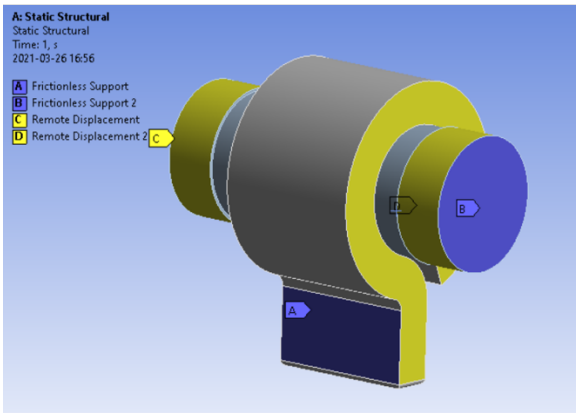

(b) *Boundary conditions for 3D analysis.*

Figure 5.12: *3D analysis.*

Mesh

The mesh is created to primarily have only Hexa elements to reduce the number of elements and hence speed up the simulation. For the same maximum element size, a Hexahedral element occupies more volume than a tetrahedral element, hence fewer elements are needed to generate the final mesh. Fewer elements can reduce the simulations time. The mesh is created with each element having a maximum size of 0.3 mm for the POS, and a maximum size of 0.5 mm for the shaft. A shorter version of the shaft is used as only one POS is to be simulated. Even at this mesh density, the 3D analysis has around 68,479 nodes and 14,564 elements. This high number of elements is one of the potential reasons for the long solution time. A point of focus for the simulations conducted further on in this project is to optimize the mesh so that the number of elements reduces. Shorter solution times are beneficial for iterating the model.

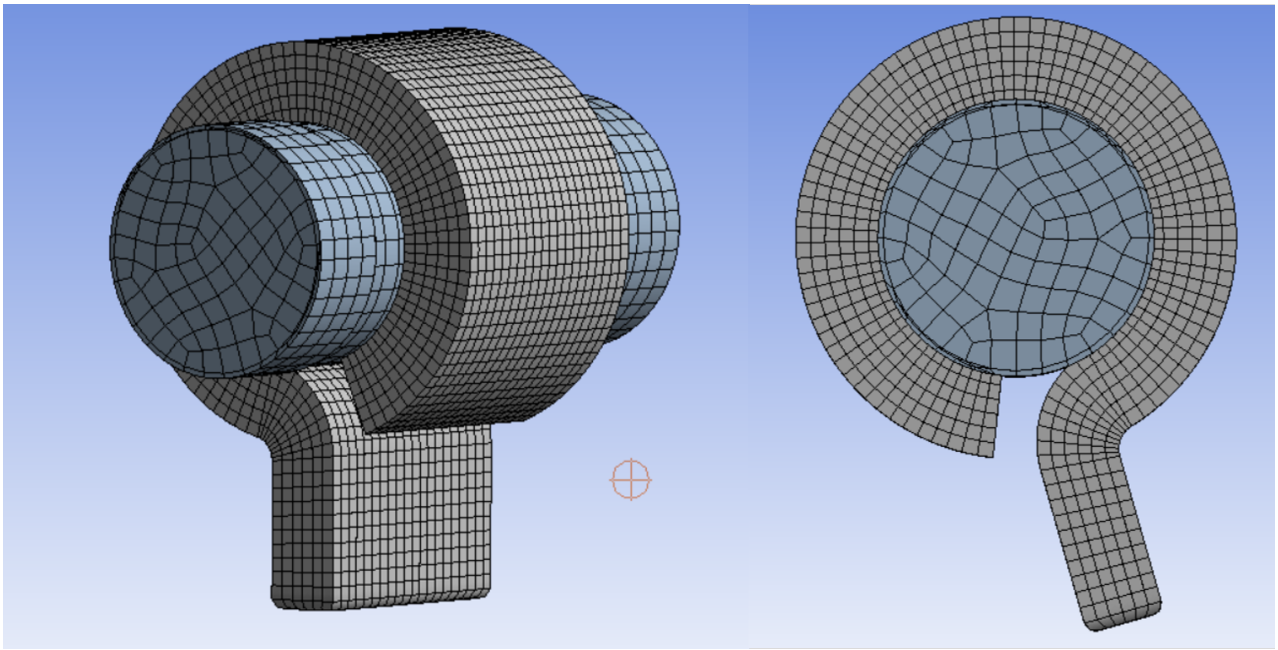

Figure 5.13: *3D analysis mesh.*

Results

The stress distribution and deformation are close to the results for the 2D simulations. The stress (Figure 5.14) follows the same pattern of a beam in bending with the stress values comparable to the 2D simulations. The deformation is also comparable, with only a 0.03 mm difference between the 2D and 3D simulations. The deformation can be seen in Figure 5.15.

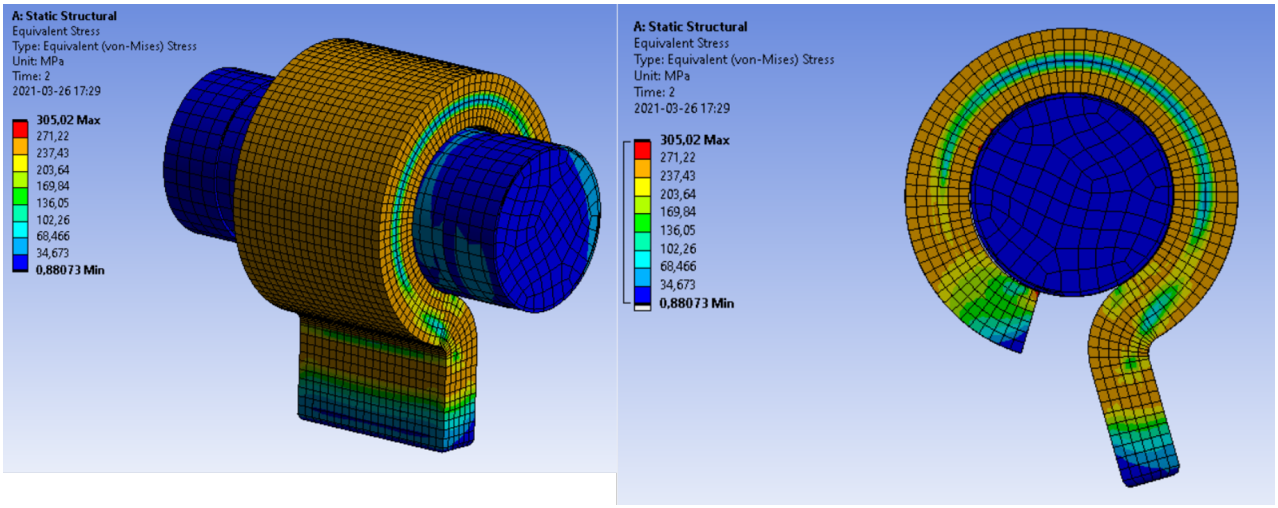

Figure 5.14: *3D analysis stress distribution.*

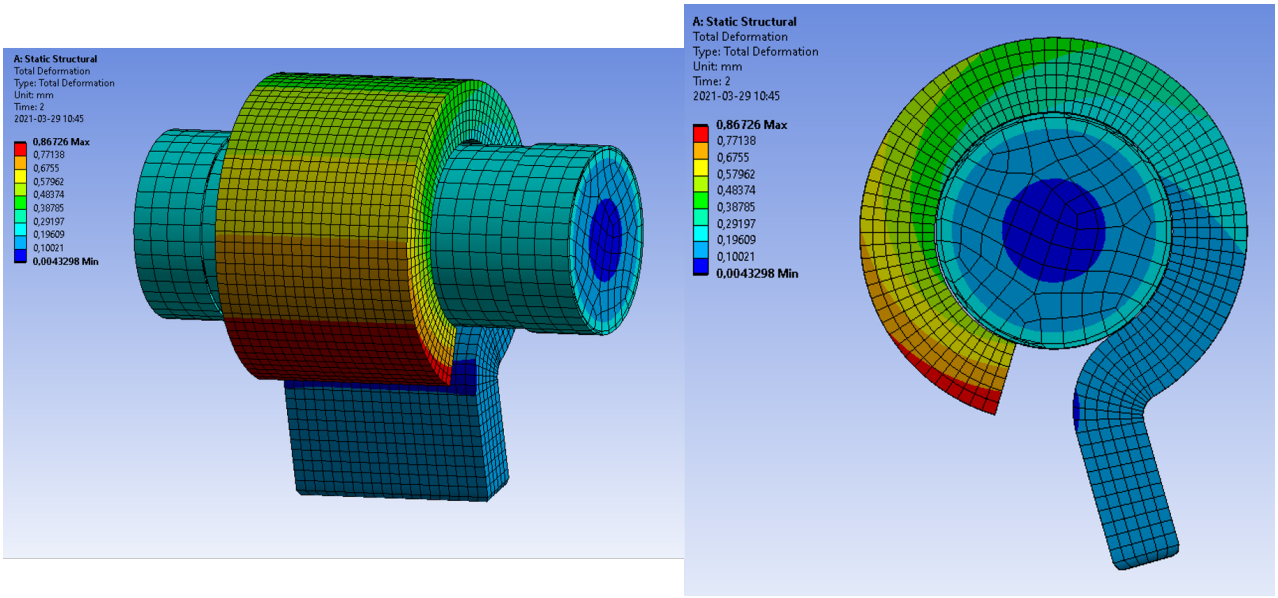

Figure 5.15: *3D analysis deformation.*

The pressure distribution, however, has an interesting pattern: from the side view the pressure distribution is as expected and as seen in the 2D simulation, but it is evident that the pressure is not uniform across the thickness. It is focused on the outer edges of the POS, with the middle portions of the thickness showing negligible pressure. This pattern of pressure distribution can produce some changes to the torque acting on the shaft.

The torque plot for 3D analysis is shown in Figure 5.17. Overall, the torque values seen in the 2D and 3D are comparable, with 2D showing a maximum torque of 427.84N mm and 468.8Nmm in the 3D analysis. The higher torque in 3D can be attributed to the higher contact pressure.

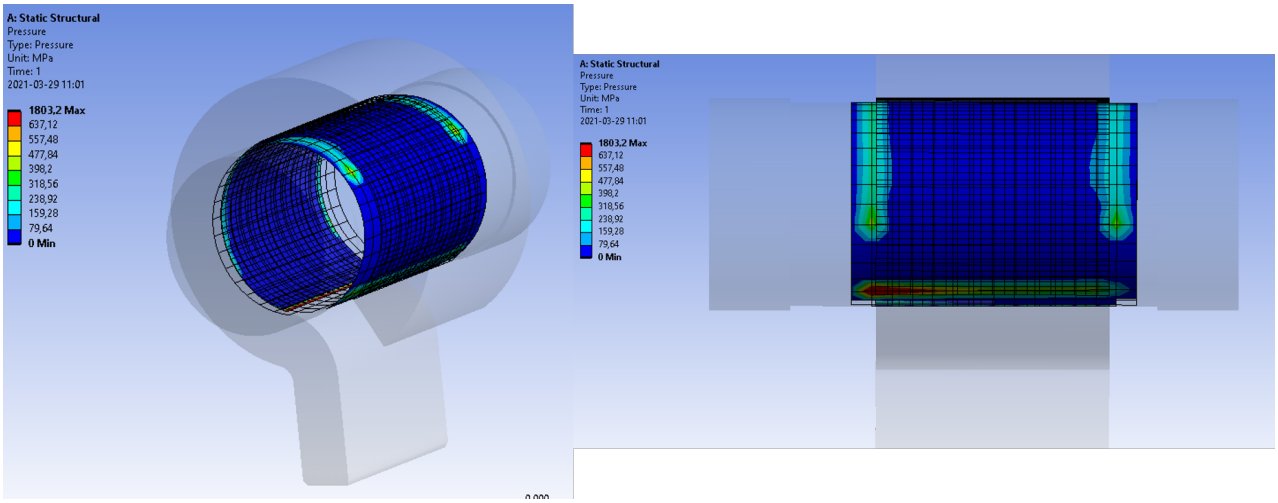

Figure 5.16: *3D analysis pressure distribution.*

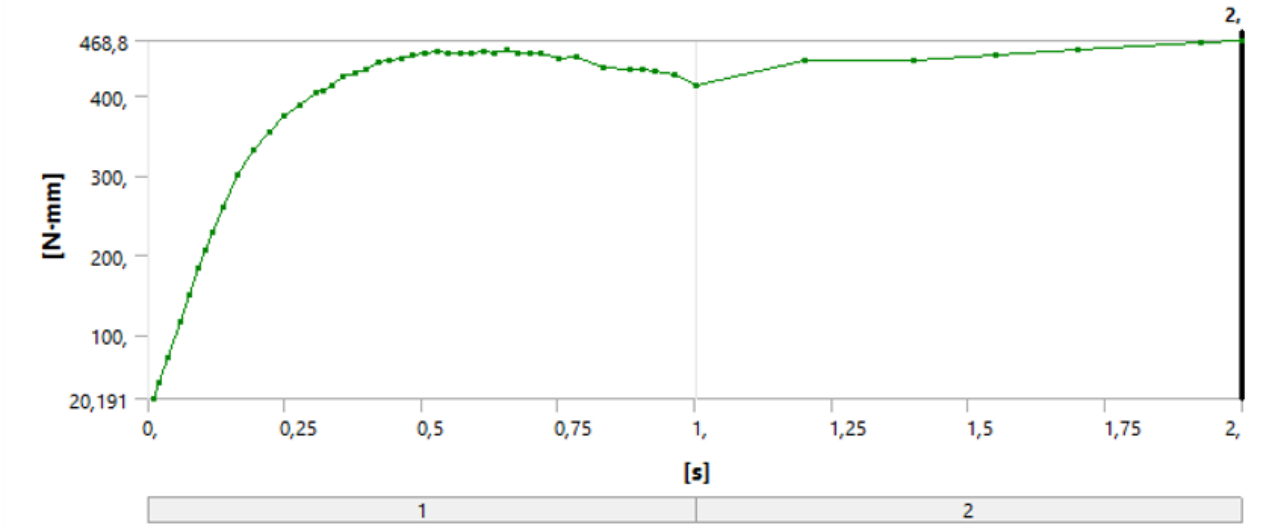

Figure 5.17: *3D analysis moment reaction.*

Reflections

The studies described above helped to get a lot of insight into ANSYS and the problem at hand. It also highlighted the differences between a 2D and 3D simulation. The 2D analysis can be very effective with simulation times close to 15-30 min. However, the assumption that the distribution of pressure is spread out evenly throughout the width of the part may not be entirely accurate for this problem. While 3D simulations are more trustworthy and provides greater resolution of data, it takes from 4 up to 78 hours to solve, which makes them inefficient to run multiple iterations. It is important to note that these FEM models do not have optimized mesh or parameters, so the solution time might decrease for further simulations conducted in this project.

Another issue is the choice of boundary conditions - in reality, the POS is not locked when the interference fit is created, yet the FEM results showed a significant torque acting on the shaft during this period, but this should be absent during the hinge operation. Hence it is important that once this initial torque is eliminated from the simulation, the model behavior may fit closer to reality.

When the torque values are compared against the initial tests that were carried out by IKEA, it can be observed that the torque seen in the experiments is roughly twice the values seen in the simulations. Thus for the iterations seen in Section **??**, a friction coefficient of 0.2 will be considered. This should give us approximately double torque values.

5.2 Refined Simulations

For the next set of simulations, the boundary conditions are changed so that they better reflect reality. The aim is to allow the POS to expand unconstrained, and then lock its rotation after the interference is normalized. At the same time, the mesh is optimized for lower solution times.

5.2.1 2D Analysis iteration 2

The main focus of this test is to allow the POS to expand without restrictions. This would eliminate the torque acting on the shaft due to the expansion of the POS. The basic geometry and analysis settings are retained from the previous iteration. A few changes are made to fix the nonrealistic behaviors noticed in the previous model iteration. The details are described in the sections below.

Geometry

The geometry for this analysis consists of the shaft, the POS, and a third body (later referred to as the Stop), which restricts the movement of the POS when required. The geometry can be found in Figure 5.18. The Stop is designed to have a wider gap than the middle part of the hinge has in reality because the POS should have sufficient room to expand in the first time step.

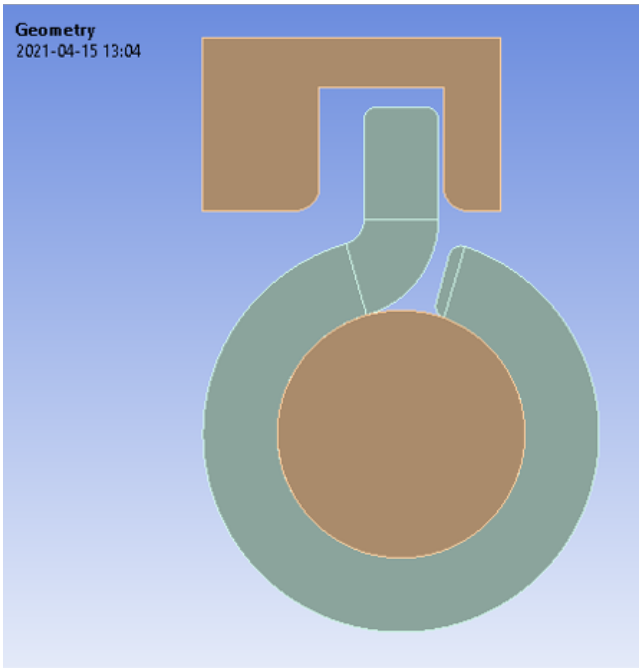

Figure 5.18: *2D analysis, iteration 2 Geometry.*

Boundary conditions

The POS is not restricted by any boundary conditions. Instead, it is controlled solely by the contacts. The first one is between the surface of the shaft and the inner surface of the POS (a frictional contact with the coefficient of friction of 0.2). The second and third contacts are formed between the extended arm of the POS and the inner surfaces of the Stop (Figure 5.19b). The contacts with the Stop are frictionless as they are used only to restrict the motion of POS. The shaft has one frictionless support to prevent motion along the Y-axis and a remote displacement applied across the circumference of the shaft to control the rotation that restricts the movement of the shaft along the X- and Y-axis and controls the rotation of the shaft in steps as seen in Figure 5.20.

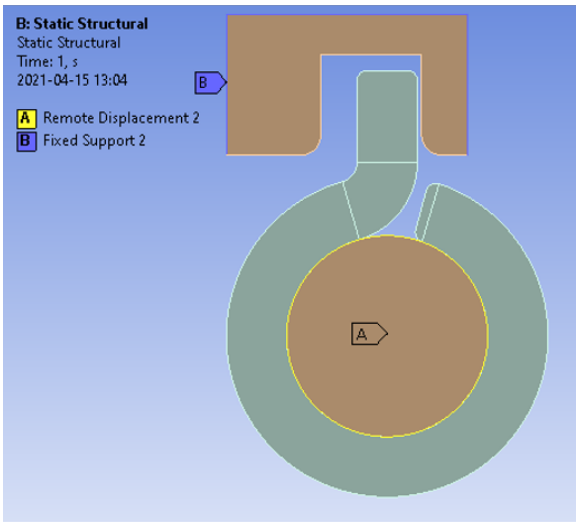

(a) *2D analysis, iteration 2 Boundary conditions.*

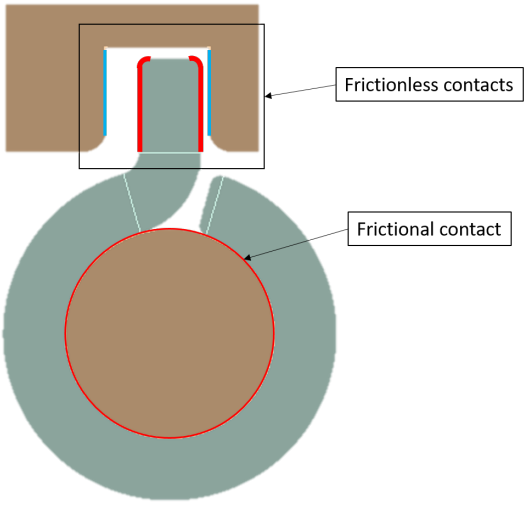

(b) *Contact formulation.*

Figure 5.19: *2D analysis, iteration 2 setup.*

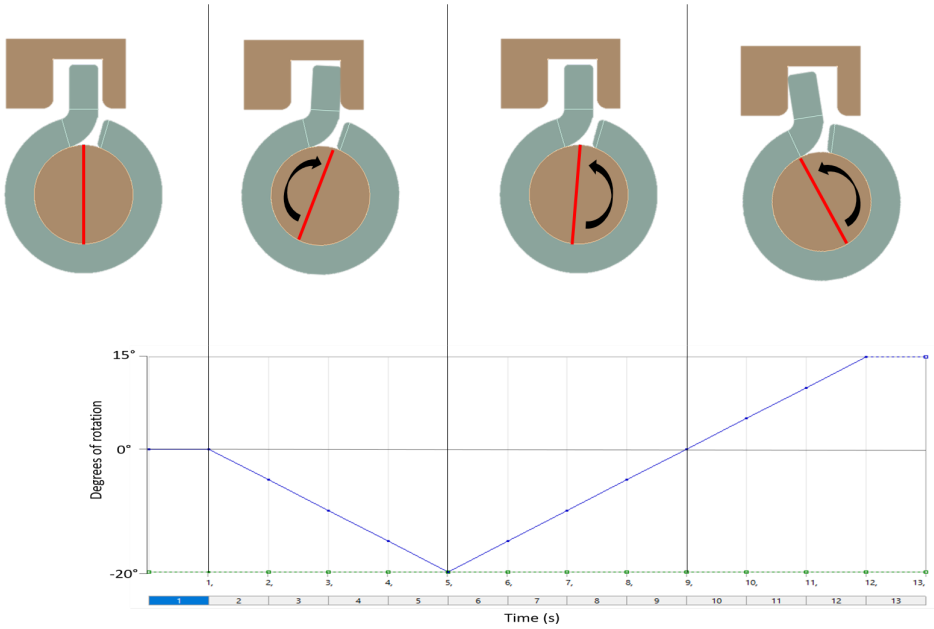

Figure 5.20: *2D analysis, iteration 2 remote displacement.*

Mesh

The mesh for this iteration (Figure 5.21) is optimised to improve solution times. The main focus is to keep the mesh density high in areas of interest, but have a coarse mesh where stress and deformations are low.

The mesh for the shaft is a quad-dominant mesh with inflation added to the surface to ensure that at the surface the mesh density is high, but will reduce towards the center of the shaft. The mesh for the POS is also quad dominant, but the meshing method is quite different. The surface of the POS is split up into smaller sections which allow each section to be meshed separately enabling an even face mesh across most of the POS. For the mesh of the Stop, inflation is added to the edges in contact with POS.

Additionally the rounded edges that have contacts assigned to them are split up into multiple elements to improve the quality of the result. The optimised mesh also significantly lowers the number of elements, making the simulation computationally cheaper.

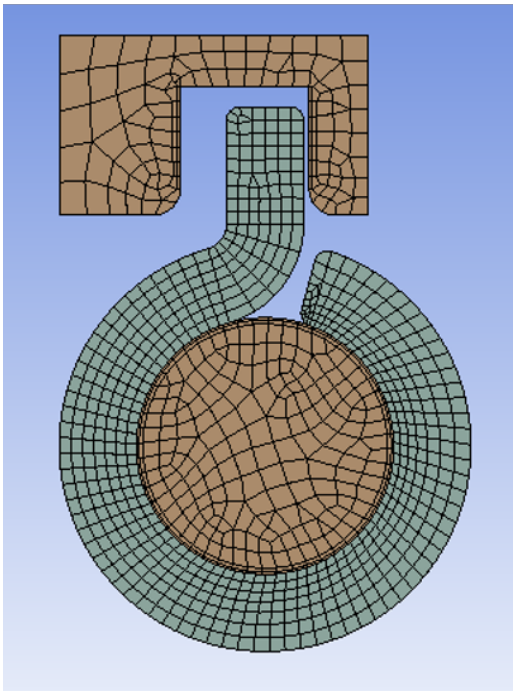

Figure 5.21: *2D analysis iteration 2 mesh.*

Results

The stress distribution for this iteration is shown in Figure 5.22. Though the stress distribution in the POS is similar to the one seen in the first iteration, the trend seen in the moment reaction seems realistic. Since the POS expands without any resistance, there exists no moment reaction for the initial step, but as the shaft is rotated, the POS rotates with it until it comes in contact with the Stop. The contact status and torque curves are seen in Figure 5.23 confirm the behavior of the model with reality - torque is induced on the shaft only when the POS is in contact with the Stop. We see a higher torque (about 749 Nmm) when the shaft is rotated clockwise, and around half of it (about 343 Nmm) in the anticlockwise direction.

5.2.2 3D analysis iteration 2

Once the idea of introducing the Stop was assessed using the 2D analysis, the same was repeated with the 3D analysis to compare the two models.

Geometry

The geometry selected for this test is the same as the one for the first iteration. The Stop has the same dimensions as the 2D analysis and is created with a sufficient gap to accommodate the expansion of the POS. The geometry is shown in Figure 5.24. The 3D POS, however, has to be split into 3 separate bodies, to facilitate better meshing. It is split up as shown in Figure 5.24. The bodies are bonded together by using bonded contact.

Boundary conditions

The boundary conditions are exactly the same as the 2D analysis: the POS is only restricted by the contacts and the shaft is controlled by a remote displacement. The load pattern for the remote displacement is shown in Figure 5.25b. The outer edges of the shaft have fixed support applied to them.

Mesh

A sensitive aspect of the mesh for the 3D analysis is that altering the number of elements introduces a trade-off between the solution time and the quality of results. Thus it is important to have a sufficiently fine mesh at

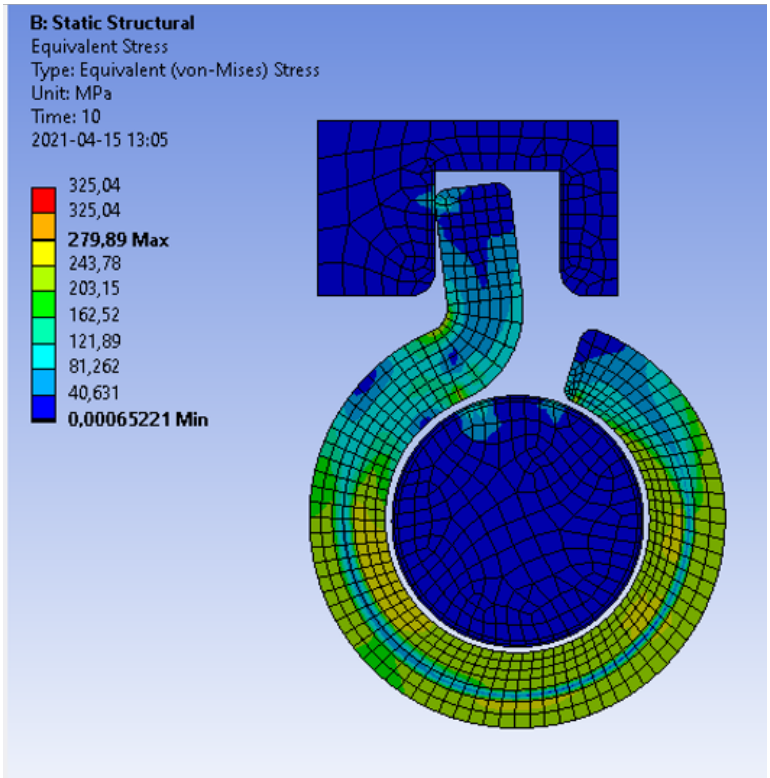

Figure 5.22: *2D analysis iteration 2 Stress distribution.*

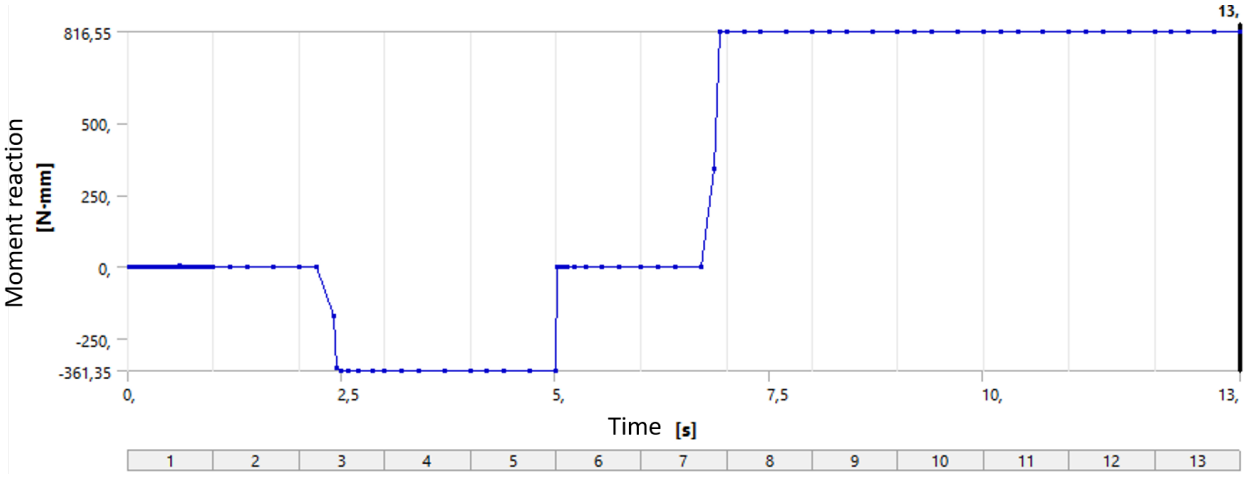

Figure 5.23: *2D analysis iteration 2 Torque curve.*

the critical areas, but ensure that areas that are not of interest are coarsely meshed. Otherwise, the solution times for the model can be too large to be of practical use.

The mesh for the shaft is a hex dominant mesh, with inflation added to the circumference. Since the POS is split into 3 bodies, the meshing becomes easier. All three bodies have a hex dominant mesh, but the large middle section is additionally face meshed to get a smooth and symmetric mesh structure. The critical areas of the POS have denser mesh (obtained by e.g. forcing number of divisions on the edge), but overall the element size is relatively large with maximum element size of 0.4 mm. The final mesh is shown in Figure 5.26.

Results

The stress distribution is in inline with the expected behavior. The torque curves are also as per the 2D analysis, though a slightly higher torque is observed than in the 2D analysis. This can be explained by the

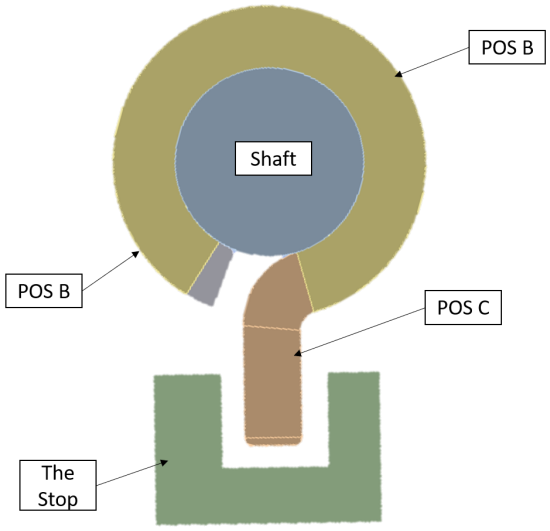

Figure 5.24: *3D analysis iteration 2 Geometry.*

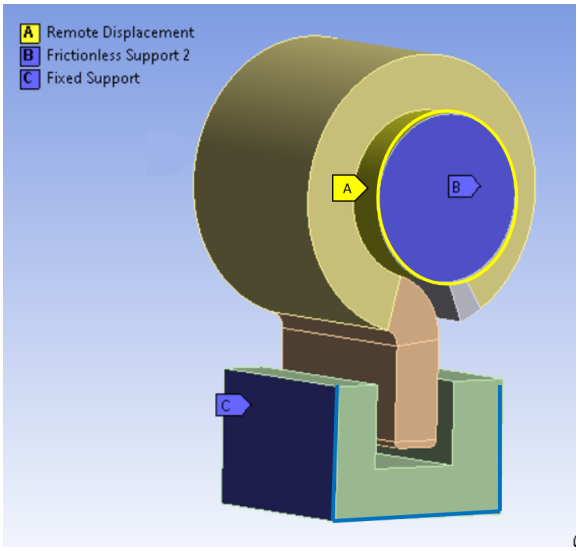

(a) *3D analysis iteration 2 Boundary conditions.*

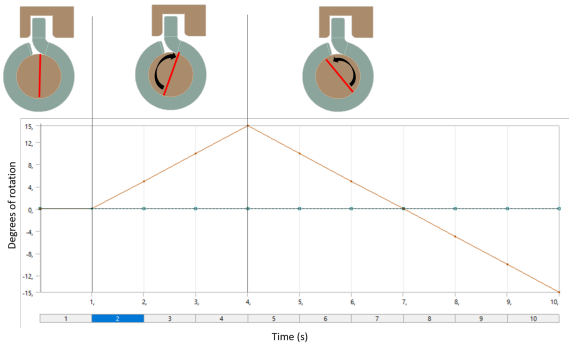

(b) *Remote displacement setup.*

Figure 5.25: *3D analysis iteration 2 setup.*

higher contact pressure values. In 2D analysis, the contact pressure is distributed across the thickness of the POS, whereas in the 3D analysis the pressure is concentrated at the outer edges of the POS. Assuming the same force is exerted by the expansion of the POS since the contact area is smaller in the 3D, the higher contact pressure is observed.

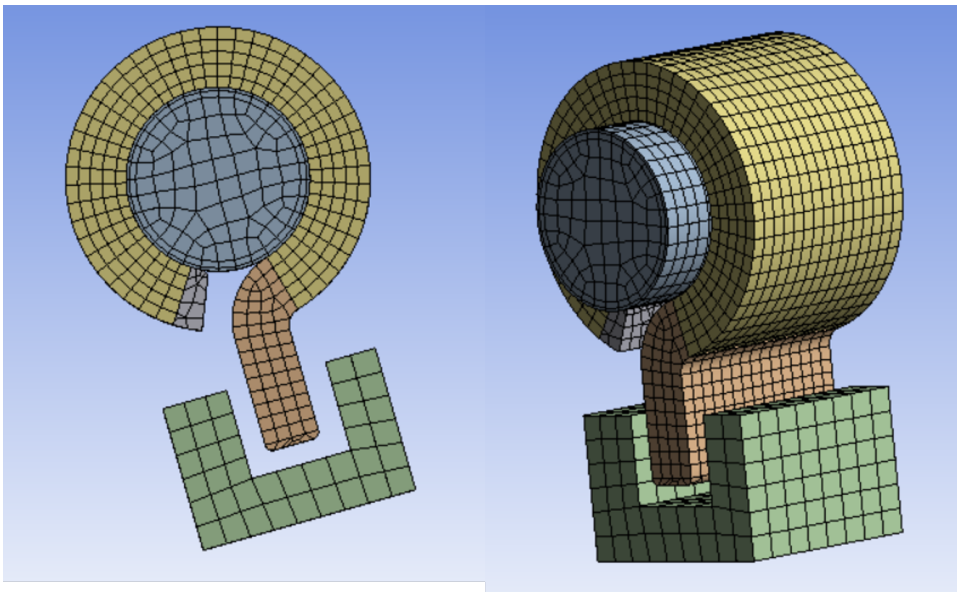

Figure 5.26: *3D analysis iteration 2 Mesh.*

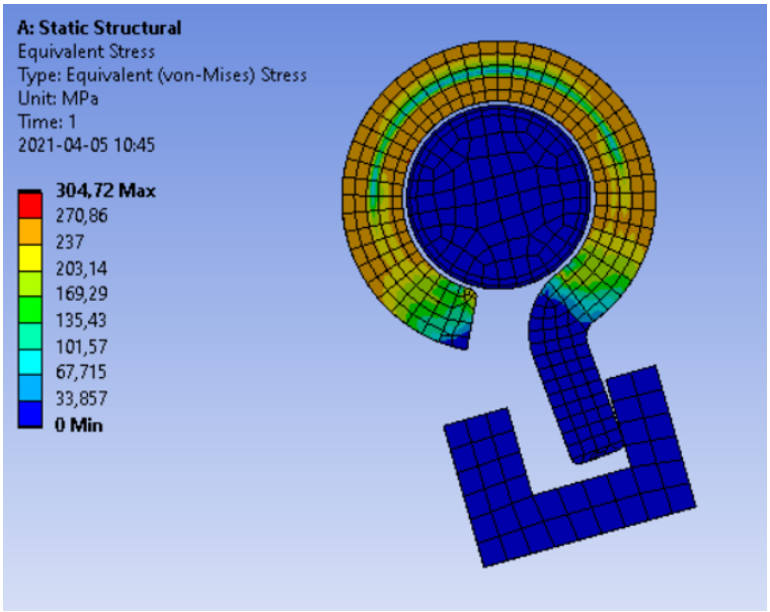

Figure 5.27: *3D analysis iteration 2 Stress distribution.*

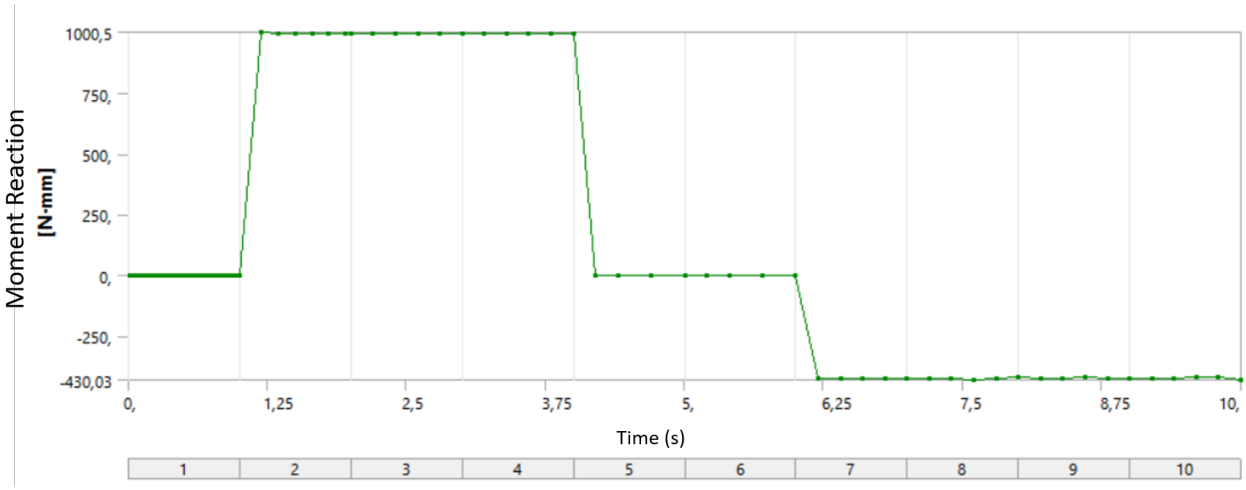

Figure 5.28: *3D analysis iteration 2 Moment reaction.*

6 Results

This chapter of the report focuses on the results of the project. The first section covers the findings from the Finite Element study alone, the second one - from the experiments on prototypes, while the third part deals with the learning's that come from combining the experimental and FEM studies.

6.1 Finite Element Analysis

The main goal of the project was to develop guidelines for modeling the friction hinge in FEM software. Below general instructions as to how to do so are presented. The instruction presented are generalized to explain the cause and reason behind them. This is an attempt to keep the instructions independent of the FEM software package. Some sections are more software-specific than others. To translate these settings from ANSYS to designated software please refer to ANSYS User Guide [27].

6.1.1 FE Modelling procedure for friction hinge in ANSYS

1. Geometry and Materials
   - Verify materials assigned
     - Part on Shaft - Steel 316L
     - Shaft and Stop -HSS
2. Connections and Contacts
   - Create connection between Shaft and POS
     - Contact - Shaft, Target - POS
     - Contact type - Frictional, coefficient of friction - 0.2 (or as required)
     - Detection method - nodal to nodal projection
     - Geometric modifications - add offset, ramping effects, desired radial interference
   - Create connection between Shaft and Stop
     - Contact - Shaft, Target - Stop
     - Contact type - Frictionless
     - Pinball radius - large, (at least the distance of the gap)
3. Mesh
   - Shaft
     - Insert mesh method > Multizone > Hexa, element size 0.5mm
     - Insert inflation > Boundary condition (Figure 6.1 area C)
     - Body sizing - 0.5mm
   - POS
     - Insert mesh method > Multizone > Hexa, element size 0.5mm, scooping method - front face of POS
     - Body sizing - 0.4mm
     - Edge sizing > Across thickness (Figure 6.1 area B) > Number of divisions 5 (the number of elements across thickness of POS. If number of divisions is high it may be required to decrease element size in body sizing
     - Edge sizing > On corners (Figure 6.1 area A) > Number of divisions 4
   - Stop
     - Add body sizing if needed to mach the element size to the POS
4. Analysis

- Analysis settings
  - Large deflections >on
  - Weak springs > on
  - Adjust number of steps
- Boundary conditions
  - Stop: Fix outer edges
  - Shaft: remote displacement on the outer surface. All degrees of freedom except form rotation around cylinder axis = 0. Rotation around cylinder axis - step 1 = 0 (pure expansion of POS), step 2+ =/= 0. Frictionless support on one of the sides

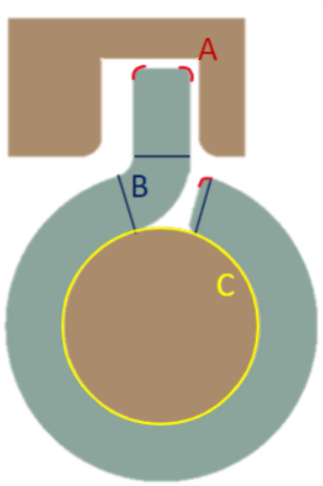

Figure 6.1: *The hinge model with areas referenced in the guide marked.*

A model created as explained above produces reasonable, physical results, but its largest disadvantage is relatively long computing time (3-5 hours). It was not convenient to use this model while performing several simulations in a row to study the influence of a specific parameter on the torque. Therefore, a comparison between 2D and 3D simulation results was made using a model with the Stop. The results for four different thickness dimensions for POS were calculated and combined. It was decided that to say the 2D approximation is acceptable to be used in later studies the error should not exceed +/-10%. The graph in Figure 6.2 presents the result of the study. Gray areas are +/-10% error bands. As it can be observed, the simplified model fulfills the requirements.

One of the parameters that were examined by running several simulations for different values was the coefficient of friction. A 2D model with Stop was used to calculate torque values for various coefficients of friction ranging from 0.18 to 0.23. An example of the results from such a study for a part on shaft THK C can be found in Figure 6.3.

This study not only shows the nature of the relationship between the coefficient of friction and the torque but also allowed to find a function that gives a good approximation of the coefficient of friction for given torque. The experimental data set has the torque values and coefficient of friction in an unknown, but in the FEM model, the coefficient of friction is the input. Therefore, when calibrating the FEM model to experimental results such approximation allows to quickly find the desired coefficient of friction and aids in quick calibration.

6.2 Experimental results

Based on the initial studies and FEM simulations the samples described in Table 4.3 were ordered. The torque required to rotate the shaft was measured after each POS was assembled on the shaft. The torque was measured with the method described in Section 4.3.1. As described in Section 4.3 multiple samples of the same specifications are ordered. this was to check if the samples produced consistent results with the same parameters. This section will describe the methodology of analyzing the data generated and the observations made. The individual results of each sample are captured in Appendix B.

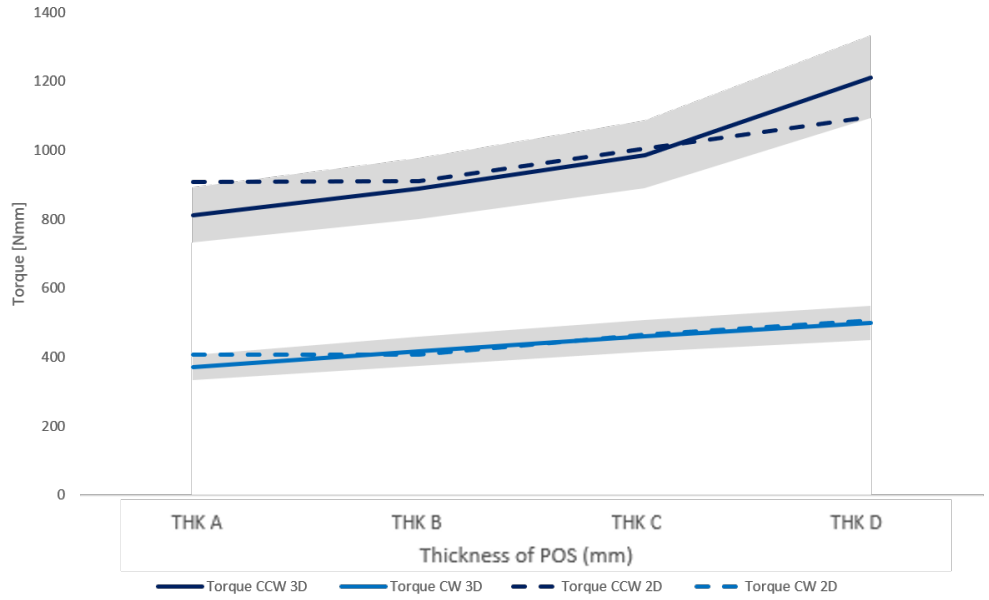

Figure 6.2: *A 2D and 3D model comparison with +/-10% from 3D results error bands.*

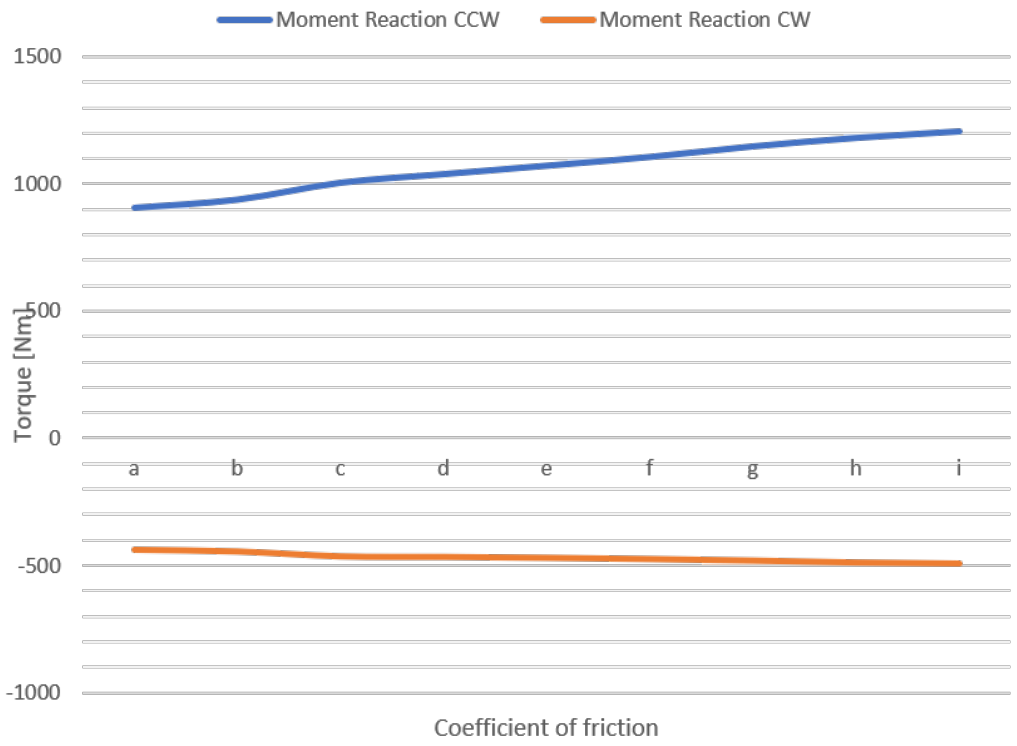

Figure 6.3: *A relation between the coefficient of friction and the torque for POS thickness THK C.*

6.2.1 Data Analysis methodology

The raw measurement data is difficult to interpret and identify trends from, therefore some post-processing must be conducted to identify the trends and make sense of the values.

The sample post-processing is described in this section, this same procedure has been followed for all the

samples.

Raw data

The data collected by the supplier, without any form of processing is the raw data, is shown in Table 6.1. This Table describe the data for Scenario 2.

The first column of the table denotes the rotation direction (CW or CCW) and the assembly direction L or R as described in Section 2.

CW	Shaft 1 Torque (Kg x mm)	Shaft 2 Torque (Kg x mm)	Shaft 3 Torque (Kg x mm)
L	100	90	105
LL	210	180	210
LLL	300	260	325
LLLR	520	480	500
CCW	Shaft 1 Torque (Kg x mm)	Shaft 2 Torque (Kg x mm)	Shaft 3 Torque (Kg x mm)
L	180	162,5	165
LL	310	370	330
LLL	500	475	500
LLLR	650	600	640

Table 6.1: Raw data Sample.

The first step is to convert the unit of torque to Nmm, to standardise the unit of measurement. Thus multiplying the torque values by 9.8. The next step is to calculate the multiplier, i.e we calculate the contribution of each POS to the torque in comparison to the first POS that was assembled on the shaft. To do this we use the equation $m = (T_{n,\text{dir}} - T_{n-1,\text{dir}})/T_{1,\text{dir}}$ The difference in torque before and after the addition of a POS is divided by the torque of a single POS added in the respective rotation direction.

A sample of the multipliers is shown in Table 6.2.

CW	**shaft 1** Torque (N x mm)	**Multiplier**	**shaft 2** Torque (N x mm)	**Multiplier**	**shaft 3** Torque (N x mm)	**Multiplier**
L	980.00		882.00		1029.00	
LL	2058.00	1.10	1764.00	1.00	2058.00	1.00
LLL	2940.00	0.90	2548.00	0.89	3185.00	1.10
LLLR	5096.00	1.22	4704.00	1.35	4900.00	1.06
CCW	**shaft 1** Torque (N x mm)	**Multiplier**	**shaft 2** Torque (N x mm)	**Multiplier**	**shaft 3** Torque (N x mm)	**Multiplier**
L	1764.00		1592.50		1617.00	
LL	3038.00	0.72	3626.00	1.28	3234.00	1.00
LLL	4900.00	1.06	4655.00	0.65	4900.00	1.03
LLLR	6370.00	1.50	5880.00	1.39	6272.00	1.33

Table 6.2: Torque measurement Sample 2.

Ideally, the multiplier values should always be 1, But from the Table 6.2 it is evident that the multiplier values are varying. However for the sample described the values are quite close to 1, they vary significantly for other samples. The average torque of the 1st POS in each of the configurations is plotted in the Figure 6.4 and Figure 6.5.

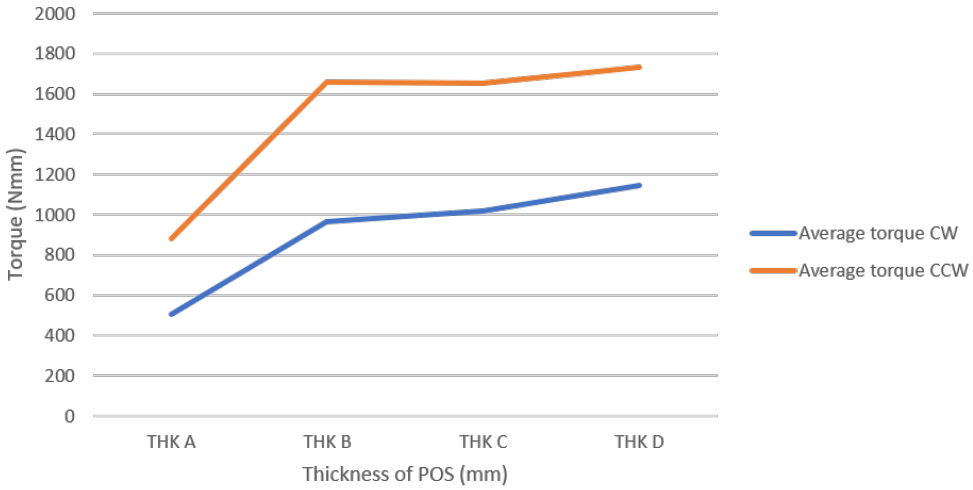

Figure 6.4: *Plot of Average torque of 1st POS vs THK.*

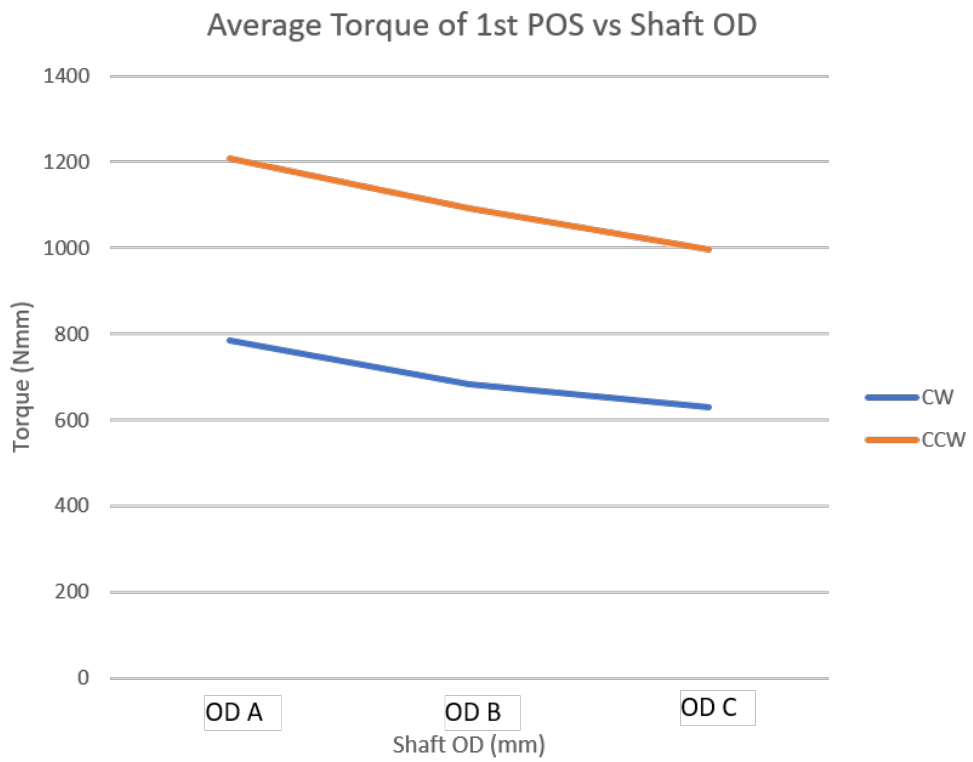

Figure 6.5: *Plot of Average torque of 1st POS vs Shaft OD.*

The next step is to calculate the increments in torque when each POS is added. This is done by simply subtracting the torque value before and after the addition of each POS and arranging the torque according to the direction of rotation based on assembly orientation. Table 6.3 shows the increments for a data sample.

Increments					
Shaft 1		Shaft 2		Shaft 3	
CW	CCW	CW	CCW	CW	CCW
980.00	1764.00	882.00	1592.50	1029.00	1617.00
1078.00	1274.00	882.00	2033.50	1029.00	1617.00
882.00	1862.00	784.00	1029.00	1127.00	1666.00
1470.00	2156.00	1225.00	2156.00	1372.00	1715.00

Table 6.3: Increments Sample.

The increments are not the same, hence calibrating a FEM model to fit any one of the increment values would produce a model with high error values, hence we average the increments. Thus for the sample shown in this section, the average values are 1062 Nmm in the CW direction and 1707 Nmm in the CCW direction.

The plots for average increments show how each configuration influences the torque. The Figure 6.6 shows the influence of THK to the increments and the Figure 6.7 is a plot of the increments vs the OD of the shaft.

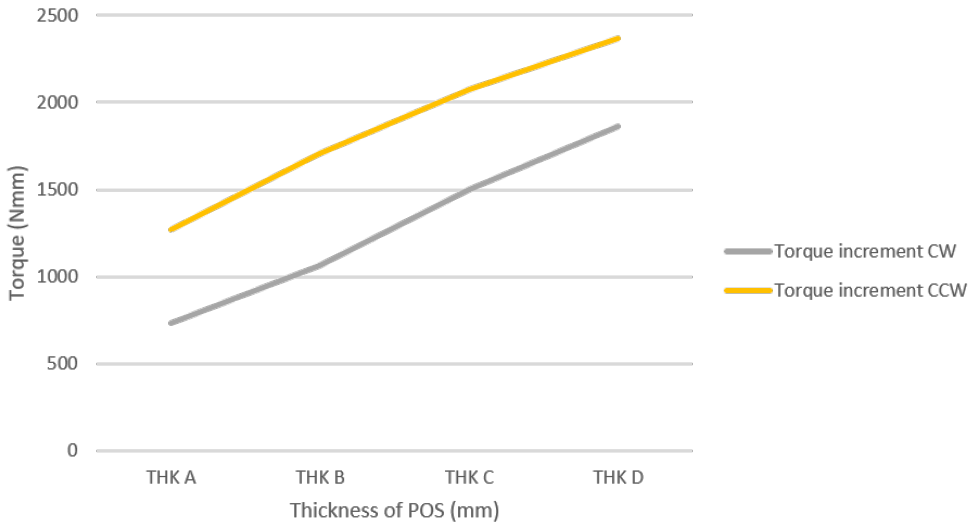

Figure 6.6: *Plot of increments vs THK.*

From the data, it is clear that there is a distinct difference in values of torque between the 1st POS and the average increments. The plot of increments shows a consistent relation between the torque and the Values of thickness and outer diameter. Whereas the average of the 1st POS does not exhibit a strong trend. This phenomenon is discussed further in the calibration section.

6.3 Combining FEM model and experiment results

In this section post processing of data is described along with the process of calibrating the FEM model to a sample empirical data is described. The calibrated FEM model is then validated against the remaining empirical data. lastly the conclusions from the validation are discussed.

6.3.1 Calibration of FEM model

The FEM model described in Section 5, was built to represent the real-life conditions, the simulations carried out in the chapter 5 verified the behavior of the model with experimental observations, it was however not calibrated to represent the actual values seen in the prototypes. In this section, the process of calibrating the FEM model to the experimental data is described. There are two parameters to calibrate the friction coefficient and the boundary condition applied to the POS.

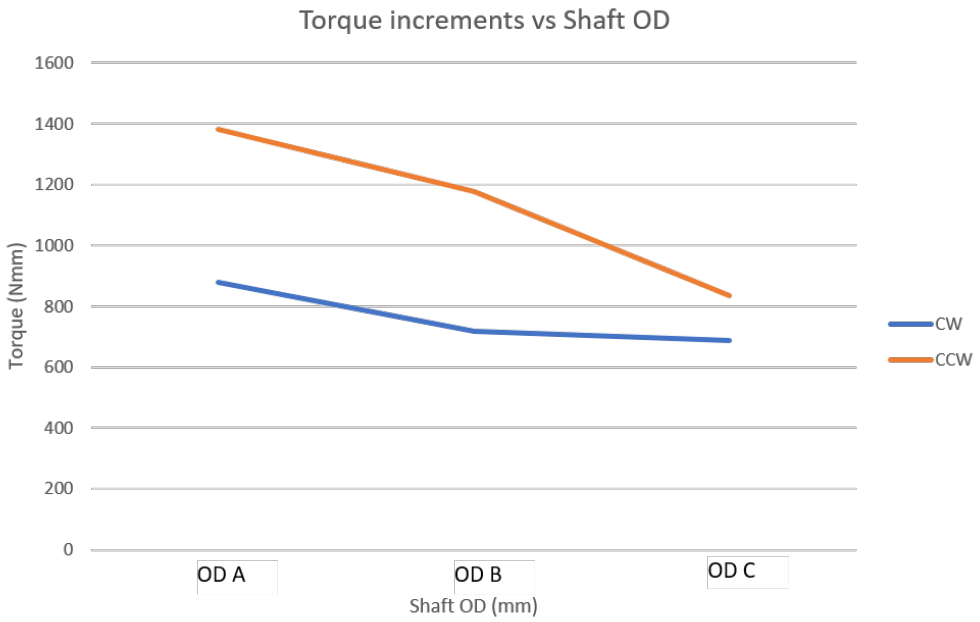

Figure 6.7: *Plot of increments vs Shaft OD.*

Coefficient of friction

In the FEM model simulations the coefficient of friction was assumed during the verification stage, as not have enough data was available to know the exact friction coefficient of the two surfaces in contact. But using the data captured from prototypes shown in Appendix B. We can approximate the coefficient of friction.

To calibrate the model, the data from an assembly with a POS of THK C was used. This was selected because 5 samples of this configuration were manufactured, We also see that the average deviation of torque values for this sample is low. Using the relation shown in Figure 6.3 we can estimate the friction coefficient.

Boundary condition

The test setup for the experiments can be seen in Figure 6.8. The instrument used to measure the force is a dynamometer.

From the figure, we can infer the boundary conditions that may be closest to this scenario. We can clearly see that the POS in the shaft assembly is clamped in place. This setup closely resembles the boundary condition when the POS is held in place by fixed support (BC1). However by intuition the boundary condition with the 3rd body, ie the Stop (BC2) is closer to the actual hinge in operation. Additionally, if the shaft assembly is observed, the shaft is not supported by any other means but the POS i.e in effect the shaft is allowed to move in all directions and is held only by the contact. This was also simulated in ANSYS as BC3. The three setups are shown in Figure 6.9.

The torque values from the simulations for all three configurations were compiled and verified against the experimental setup. The values are shown in Table 6.4. It clearly shows that as expected the Fixed constraint is the closest approximation.

THK C, μ C coefficient of friction **Boundary conditions**	**Torque CW [Nmm]**	**Torque CCW [Nmm]**
Real (experiment)	1016.75	1653.75
Fixed (Clamped POS)	1334.16	1765.8
With Stop (3rd part)	510.12	1334.16
Fixed POS, Shaft is free to move	510.12	1177.2

Table 6.4: Boundary conditions study.

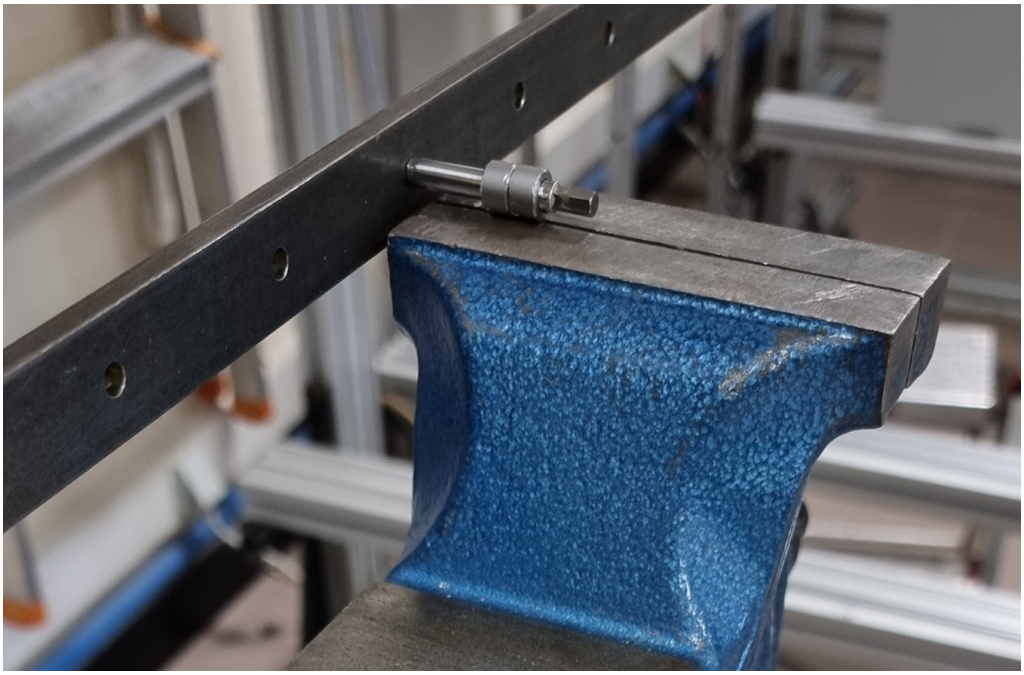

Figure 6.8: *Testing setup for measuring the torque offered by the hinge.*

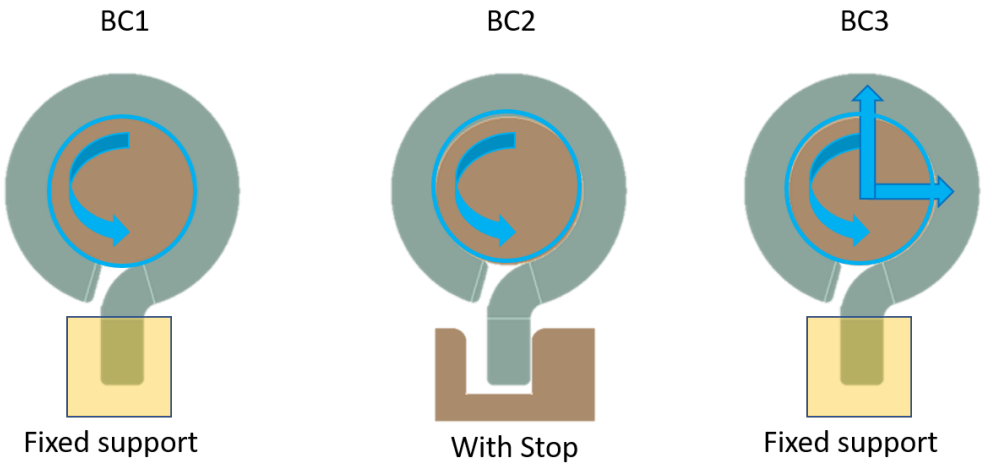

Figure 6.9: *Boundary conditions study.*

Average of 1st POS vs Average of increments

In Section 6.2.1 it is described that the data for calibration can be selected in two methods, the average torque of the 1st POS or the average increment each POS can offer. The FEM model is calibrated against both of these and the friction coefficients are noted. Table 6.5 shows the calibration values that were derived from the experiment data, and the ANSYS data generated for the respective simulation. The respective error % are also shown in the same tables.

Average 1st POS measurements			Average of the increments		
THK (mm)	**CW (Nmm)**	**CCW (Nmm)**	**THK (mm)**	**CW (Nmm)**	**CCW (Nmm)**
THK A	506	883	**THK A**	732	1301
THK B	965	1664	**THK B**	1062	1707
THK C	1018	1655	**THK C**	1501	2074
THK D	1145	1733	**THK D**	1864	2371
OD A	785	1210	**OD A**	879	1383
OD B	684	1092	**OD B**	718	1177
OD C	630	997	**OD C**	687	834

Table 6.5: Average torque of 1st POS and the average of increments in torque after assembling next POS for clockwise (CW) and counterclockwise (CCW) directions. These are the two ways of averaging the torque considered in the thesis project.

Fixed constraint vs 1st POS coeff = μ D			% error		With Stop vs 1st POS coeff = μ E			% error	
	CW (Nmm)	**CCW (Nmm)**	**CW**	**CCW**		**CW (Nmm)**	**CCW (Nmm)**	**CW**	**CCW**
THK A	1034	1522	104.3	72.3	**THK A**	473	1431	-6.5	62.1
THK B	1029	1461	6.7	-12.2	**THK B**	474	1442	-50.9	-13.4
THK C	1160	1617	13.9	-2.3	**THK C**	502	1586	-50.7	-4.2
THK D	1279	1764	11.8	1.8	**THK D**	555	1714	-51.5	-1.1
OD A	966	1359	23.0	12.3	**OD A**	421	1308	-46.4	8.2
OD B	927	1370	35.5	25.4	**OD B**	422	1328	-38.3	21.6
OD C	950	1387	50.8	39.1	**OD C**	427	1345	-32.2	34.8

Table 6.6: Table showing the ANSYS results and their respective error with respect to averages of experimental values calculated based on the torque from the 1st POS assembled.

Fixed constraint vs increments coeff = μ E			% error		With stop vs increments coeff = μ F			% error	
	CW (Nmm)	**CCW (Nmm)**	**CW**	**CCW**		**CW (Nmm)**	**CCW (Nmm)**	**CW**	**CCW**
THK A	1216	1864	66.3	43.3	**THK A**	540	2001	-26.3	53.9
THK B	1207	1854	13.6	8.6	**THK B**	579	1874	-45.5	9.8
THK C	1358	2050	-9.5	-1.1	**THK C**	677	2070	-54.9	-0.2
THK D	1488	2227	-20.2	-6.1	**THK D**	667	2453	-64.2	3.4
OD A	1105	1707	25.7	23.4	**OD A**	421	1308	-52.1	-5.4
OD B	1109	1742	54.3	48.0	**OD B**	422	1328	-41.3	12.8
OD C	1113	1771	62.1	112.4	**OD C**	427	1345	-37.9	61.3

Table 6.7: Table showing the ANSYS results and their respective error with respect to averages of experimental values based on the average increment seen in each sample.

From the error, we see that the ANSYS model with the fixed constraint is closer to the experimental values. The model was calibrated to the Scenarios 3 and 4. And the model has good accuracy for POS with THK B and THK D. Unfortunately, the values for POS with THK A do not match the ANSYS values. We have seen that even among the samples with the same configuration the torque values have very high deviation values, thus the experimental values for this configuration may be unreliable.

As for the study of the shaft with OD ID B, ID C, and ID D, The results from ANSYS show that the torque

values should be close by to each other but from the data, it is clear that the ANSYS model is over predicting the torque. The model is stiffer than expected.

But through this study, we can say that the coefficient of friction between the two materials should be around μ E, and the ANSYS model calibrated against the increments should be able to predict the torque of the final assembly with sufficient accuracy. However, the torque trend for when shaft diameter is increased could not be verified as the data did not follow the expected pattern.

6.3.2 Possible explanations

Several different hypotheses explaining the differences between the FEM and empirical results were identified. Some of them were verified later using FEM model, for example the influence of the tolerance of the outer diameter of the shaft. Other statements were left as purely theoretical discussion points and verifying them is a part of the future activities in this project.

Difference in hardness of materials

The assembly process of the prototypes involved pressing POS onto the shaft with the assembly direction for all four POS as shown in Figure 6.10. This means that the distance the POS needs to slide over the shaft decreases as new components are being added. Moreover, the hardness difference between the shaft and POS is significant with the hardness of 170-220 HV for stainless steel 316L and 700-840 HV for High-Speed Steel. This means that the contact surface of the POS may vary between the first and the last assembled part resulting in inconsistent increments of torque.

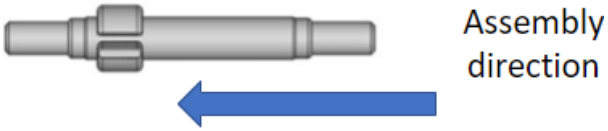

Figure 6.10: *Assembly direction of parts on shaft.*

Shaft outer diameter tolerance

Another hypothesis to be tested was how strongly the shaft diameter tolerances influence the torque result. To do so a 2D model of THK C POS thickness was run for different radial interference values. The results are plotted in Figure 6.12.

Both the clockwise and counterclockwise directional torque changes rapidly for small interference values and becomes close to constant after. After comparing these results with the maximum plastic strain it can be observed that the torque was quickly increasing only when the plastic strain was close to 0. The reason for that could be that the hardening of the material in the plastic deformation range slows down the torque increase.

Part on shaft inner diameter tolerance

Similarly, the influence of the POS inner diameter was examined. The dimension was varied from ID A to ID B with a constant outer diameter of shaft OD A. The same pattern as before was observed: low plastic strains corresponded to low and sensitive to small changes of dimension torque values, while for high strains the torque value was virtually constant. Therefore, it can be observed that the inner diameter of the part on the shaft does not have a big influence on the torque.

The last hypothesis tested was the influence of measurement method and initial wear. To do so, multiple measurements were done on two last shafts (one from Scenario 7 and Scenario 8). Results are presented in Figure 6.13. After adding each POS, measurements in both directions were made 3 times followed by a break for a few minutes this was followed by one full turn of the shaft and 3 measurements again. After this the next POS was assembled and the measurement procedure was repeated. As it can be observed in Figure 6.13, the values don't change much between the measurements. This suggests that the measurement method gives consistent results and that the variance in torque increments is not from initial wear.

6.3.3 Fatigue

The POS in the hinge assembly undergoes plastic deformation during assembly and in such a condition it is important to analyze the fatigue properties of this geometry. As a requirement, the hinge is expected to survive

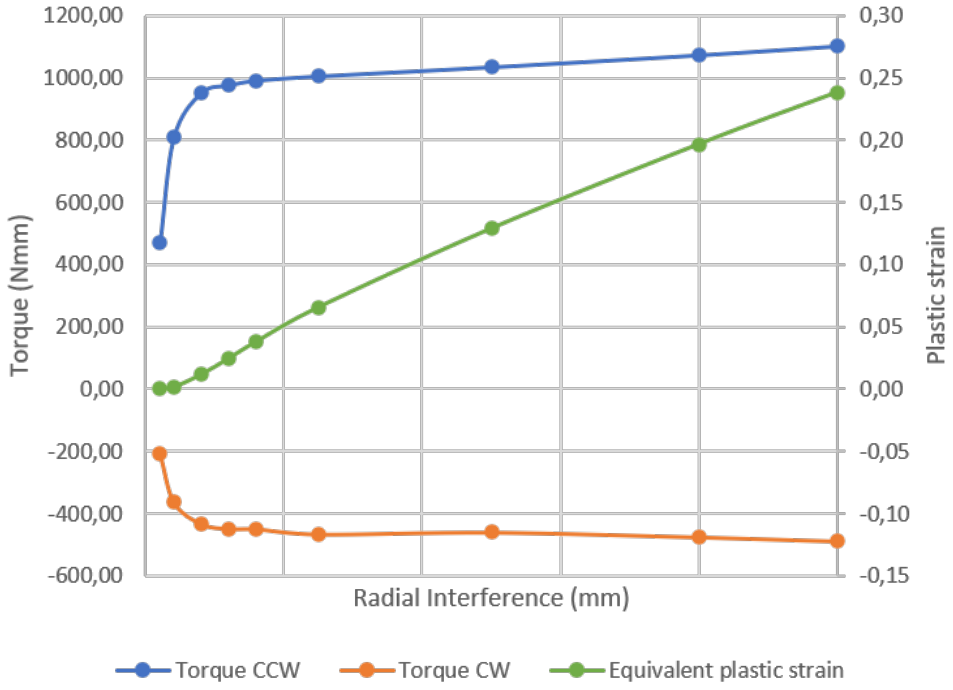

Figure 6.11: *Torque in comparison with radial interference and plastic strain.*

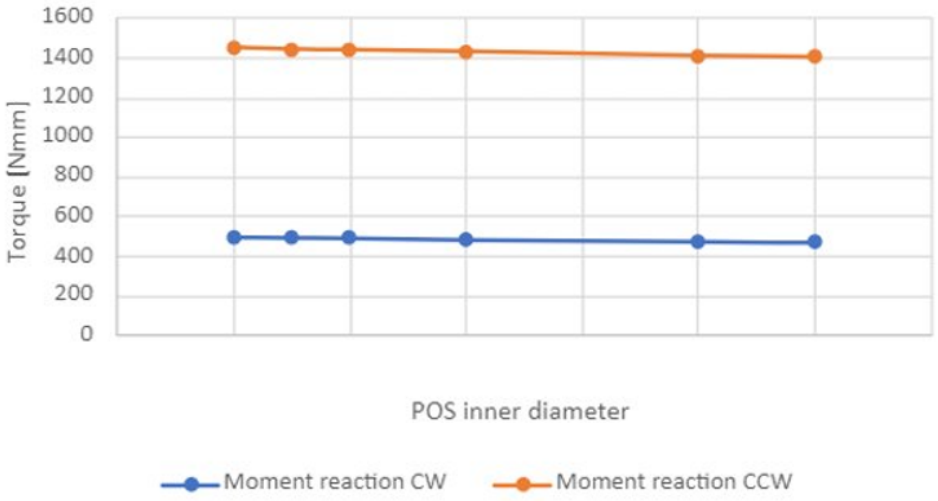

Figure 6.12: *Tolerance study with respect to POS ID.*

at least 5500 cycles of operation. Thus it is important to ensure that the hinge assembly does not experience fatigue failure in the required life cycle.

To predict the life cycle we can subject the shaft assembly to a repeated and reversed load it would experience during hinge operation. The S-N curve for stainless steel 316L was considered as per the material properties [10]. ANSYS has the option to test the fatigue life of a model based on the stress levels it is subjected to. Hence after the model was calibrated to the experimental data, a fatigue analysis was carried out. The model analyzed was the shaft assembly with the THK D POS. This was selected as this scenario showed the highest stress among the scenarios. The analysis was carried out in 3D.

From the Figure 6.14 it can be confirmed that the POS design has sufficient life when considering fatigue, The minimum life seen was about 5,750 cycles and the area of failure was the tip of the surface at the bottom of the POS (labeled with *min* in Figure 6.14). This indicates a surface failure, and the area is surrounded by

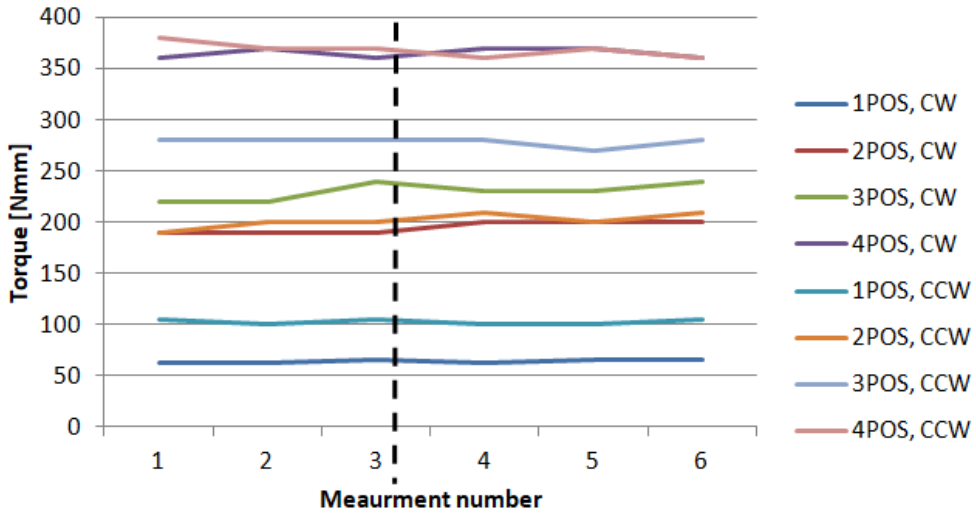

Figure 6.13: *The values of 6 consecutive measurements on the same sample and shaft (Scanario 7, Table 4.3). The measuring procedure was as follows: add one part on shaft, measure the torque 3 times with 3 minutes break after each measurement, make one full turn of the shaft (dashed vertical line), and make three more measurements with 3 minutes beaks. Assemble the next POS on the shaft.*

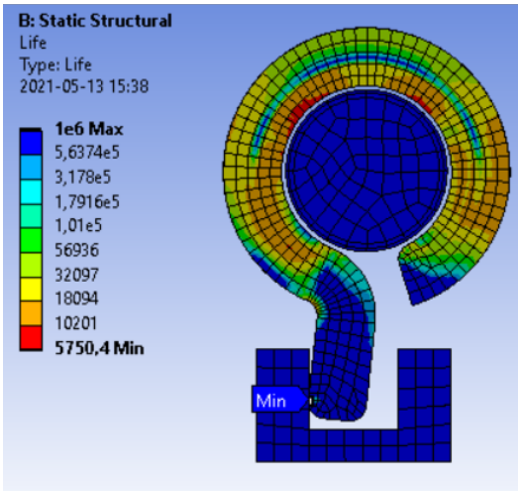

(a) *Fatigue life for a shaft assembly with THK D POS.*

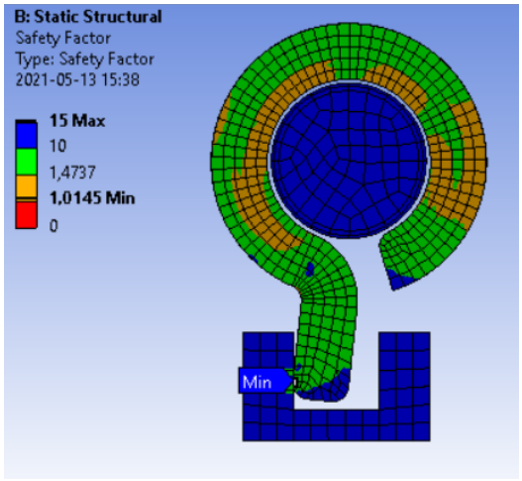

(b) *Fatigue safety factor for a shaft assembly with THK D POS.*

Figure 6.14: *Fatigue analysis.*

low-stress region, so the POS will not lose integrity because of this. However it must be noted that the factor of safety for 5500 cycles is low, so if the hinge is to be robust it must be redesigned to have a higher safety factor.

7 Conclusion

The main goal of the project was to better understand the design of friction hinges and the influence of various design parameters on torque value and performance. This was achieved with a combination of theoretical study, Finite Element Analysis, and experiments on prototypes.

Dividing the project into three aforementioned parts laid out a good, balanced workflow where each part provided a background for the next one and validated conclusions from the previous one. The theoretical study gave an overview of the market, active and inactive patents, and what kind of approximations needs to be done to find an analytical solution to the friction hinge problem. During this stage background information for the FEA study, such as materials models and potential friction coefficient, were found as well. It not only allowed for the comparison of the current hinge design against others available on market but also highlighted potentially problematic areas, such as uneven distribution of pressure on the shaft, which got confirmed during the next part of the project: the FEA analysis. This second stage was focused mainly on performing predictions of hinge behavior and improving simulation performance. These results were later validated against experimental values. The experimental study was tailored to the findings from the FEA.

The initial time schedule had to be altered slightly with the FEA part starting earlier and ending later than expected. The extended duration of this part was connected to the two biggest challenges encountered in the project: finding proper boundary conditions and a method to set up a robust and fast simulation.

Originally, it was expected that the contact definition would be the biggest issue, but thanks to using the *geometry modification* option it proved to be quite straightforward. The boundary conditions, on the other hand, took much more time than expected. Small changes in the way the hinge is constrained lead to significant changes in the torque. However, being able to use a 2D approximation instead of the 3D model with less than 10% error, as described in Section 6, considerably reduced the time to perform one simulation, allowing to make more design iterations.

Nevertheless, in the beginning, even the 2D simulations were time-consuming and often could not converge to a solution, which was leading to wastage of computational time. The convergence could be improved by creating finer mesh and switching *Large Deformation* on so that the stiffness matrix is updated every couple of iterations. Both of these solutions increase the computational power required to solve the model. Therefore, it was important to balance the robustness of the simulation and computing time. While *Large Deflections on* was a necessary option, the mesh could be changed relatively freely. Meshing was improved using a trial-and-error approach to try out different elements size, shape, and distribution, and finally, the optimal settings and adjustments needed to get the model running were identified and documented as a set of guidelines. This is documented in Section 6.1. By following these guidelines the model for this kind of simulation can be built to be robust and dependable. These guidelines were used to build FEM models for all the configurations fairly quickly and none of the later models faced convergence issues. Total simulation time for the 3D model was finally reduced to 3-4 hours from the initial 24+ hours with a good convergence rate. The developed method was robust enough to be applicable also for hinges with altered dimensions or even geometry. Due to the reduced time it was possible to investigate the influence of several different parameters on the hinge performance.

An important conclusion to note is the behavior of torque with respect to the coefficient of friction. The dependency is linear up to an extent where the relationship can be approximated to a first-order polynomial. This is useful information when calibrating the FEM model. This polynomial can be used to predict the coefficient of friction from the known torque. This is then verified by carrying out the simulation against this obtained value. Effectively eliminating the guesswork in calibration.

Once the behavior of the hinge was better known, several control parameters (shaft diameter, POS thickness, and assembly pattern) to be examined were chosen and a set of samples was manufactured. These samples were tested for torque using the measurement method described in Section 4.3.1. The new method has proved to be reliable as upon measuring the same samples multiple times it produced results with minimum deviation. It was also more efficient as it measured torque in a much larger range than the previously used setup. In conclusion, this setup is quite accurate and the measured torque range can be easily adjusted to the requirements, making it a sound measurement method for this application.

After a close analysis of the empirical data and the FEM model, a few conclusions can be drawn. It can be inferred that the FEM model could predict the torque for different POS thicknesses with less than 15% error for the model with fixed POS boundary conditions and averaging method based on the increments. However, for the rest of the methods, the errors were much higher. The data set has one outliner, i.e the POS with the thickness of THK A for which the results from the FEM model showed a high value of error to the experimental

results. This data subset also showed high variation among the samples. An average variation of 15-25% was seen among the data points of the data subset. In comparison, the data subsets for their POS thickness showed an average deviation of 1-5%. For this reason, the data from the configuration of THK A POS can be considered inaccurate.

With regards to the experiments with incremental shaft sizes, the expected pattern from the ANSYS model was to have a marginal increase in torque. However, the experimental samples showed that the torque reduced with the increase in the shaft diameter. However, the dataset available was limited, especially regarding the last sample which consisted only of one shaft, so taking into account the high variance seen in the samples, it is difficult to draw conclusions from this. It is interesting to note that FE model overestimated the torque values, i.e it assumed a stiffer matrix than what is seen with reality. This is due to discretization in FEM.

The fatigue test carried out in ANSYS shows that the shaft and POS can withstand the required 5500 cycles, but it must be noted that the factor of safety is marginal. Although since the stress in the POS is not expected to be due to fully reversible loads and the major stress is induced when the part is assembled onto the shaft, the actual life of the component should be sufficiently longer than the life as predicted by ANSYS. However, the initial life cycle analysis carried out shows that other parts such as the middle part and the hinge sides may be weak links. Nevertheless, this cannot be said for sure until either additional FEM studies are performed on these parts or a durability test is done on the components manufactured as per production spec. So far these parts were 3D printed which often can be tied to poor fatigue characteristics.

8 Discussion and future work

This section describes all the parts of the project that could not be verified experimentally or do not have sufficient data to be confirmed as conclusions, but may explain some of the phenomena observed during the experimental study and the cause behind them. With simulations carried out in static structural solvers of ANSYS, there is a major limitation to the analysis. ANSYS only calculates for one friction coefficient (set to the static friction by calibrating it to experimental values) and does not take into account the dynamic friction. Since the static friction offered is usually higher than dynamic, it will be the maximum friction. However, during the motion of the hinge the torque offered will be lower. This is an important factor to remember when choosing a hinge for a particular application. The FEM model will overestimate the friction offered and it is necessary to use a factor of safety to account for that. Alternatively, for estimation of the dynamic coefficient of friction a new experiment where the two types of friction are distinguished and measured needs to be made.

In Chapter 6 the different boundary conditions are compared and we can conclude that the fixed constraint is the closest to the experimental conditions. However, what is interesting to note is the magnitude of difference of the torque values between the FEM and experimental results based on the boundary conditions. In the clockwise direction, when using the model with the Stop, the torque values are around half of the ones measured in the current experiments. This has implications when calculating the total torque offered by the hinge. For a certain difference in torque values for one POS when calculating the torque for all four of them, the error multiplies.

It has been established through FEM studies that the torque produced by a POS, is dependent on the coefficient of friction. However, it must be noted that the coefficient of friction is not a constant material property. It depends on several factors of the system, such as load, elements geometry, material, surface roughness, and lubrication [4]. The assembly process involves pressing POS onto the shaft which most likely will influence the coefficient of friction, especially considering the high difference in material hardness (700-820 Vickers for HSS and 170-220 Vickers for Steel 316L).

The variation in torque values also raised the question of how susceptible the torque produced by the assembly is to tolerances of the individual components. To test this theory the assembly was analyzed in ANSYS with varying shaft diameter and varying inner diameter of the POS. As seen in the Chapter 6, it can be concluded that the design is fairly robust to the tolerance variation, as the torque values do not deviate to a large extend with varying interference. This also means that the torque produced by the POS cannot be easily increased with an increase in interference, which would be the case in the case of a circular ring. The split ring design requires a variety of other parameters such as the thickness of POS to increase its torque. This can be a key point to note in producing future designs which need higher or lower torque. However, more work to identify all the various parameters is required.

8.1 Future work

From the results and conclusion, it is evident that more work is needed to gain a comprehensive understanding of the friction hinge technology. Through this study, some parameters which control the torque have been analyzed and some parameters which do not have a major play have been identified. However, there are still several factors that need to be explored.

8.1.1 Wear and lubrication

The torque of a friction hinge is directly related to the friction coefficient. The friction coefficient is highly dependent on the surface characteristics of the two contact bodies. Thus the influence of wear on the friction coefficient will be an important study to carry out. This will help predict the torque throughout the lifecycle of the hinge. The current material combination in the two bodies has a substantially different surface hardness, which may play a big role in influencing wear.

Another aspect closely related to wear is lubrication. No studies were conducted during this master thesis project to determine the effects of lubrication. This is another important aspect to explore since the life of the hinge will be dependent on how well the hinge is lubricated. It will be crucial for life-cycle analysis.

Finally, it is advised to circle back to the patent study and analyze more closely some of the solutions. Among the patents several ways to ensure uniform lubrication across the thickness of the POS can be found, as well as the methods to allow for a more uniformly distributed contact pressure. The localized high pressure can

lead to higher wear in those regions, thus a more uniformly distributed contact pressure will improve the life of the hinge in addition to easier estimation of the torque offered by the hinge.

A Failure Mode and Effect Analysis

Item	Functions	Requirement	Failure Mode	Effects	Severity (1-5)
Parts on Shaft	Create interference/friction against shaft	3Nm	Slippage, loss of friction	Reduced torque	3
				Table top failed to stop	5
				Damage of hinge and table	4
	Receive torque from Mid part	3Nm (Reaction torque)	Permanent damage of the hinge (damage of parts of shaft)	Functioning is compromised, total hinge failure	4
Shaft	Bearing member	FOS >1 Axis of pivot	Failure by torsional yielding	Functioning is compromised, total hinge failure	4
	Create interference/friction against parts on shaft	3Nm	Slippage, loss of friction	Reduced torque	3
				Table top failed to stop	5
				Damage of hinge and table	4
	Facilitate movement	Smooth operation	Jammed shaft movement	Loss of movement, hence loss of functionality of table	2
			Squeaky sounds	Annoyed user, increased wear	1
Left/Right part	Connect side B to hinge	Connect via M5 screws	Screw rips out of wood	Damage of table, loss of movement	5
	Transmit torque to shaft	No slippage	Shaft and part lose connection gradually	No torque from hinge	3
Mid Part	Connect side A to hinge	Connect via M5 screws	Screw rips out of wood	Damage of table, loss of movement	5
	Transmit torque to parts on shaft	3Nm (Reaction torque)	Permanent damage of the hinge (damage of parts of shaft)	Functioning is compromised, total hinge failure	4
	Survive lifecycle	5500 operations	Integrity failure	Functioning is compromised, reduced hinge life	3

Item	Failure Mode	Effects	Control Methods	
			Prevention Control	Detection Control
Parts on Shaft	Slippage, loss of friction	Reduced torque	FEM analysis to design part with appropriate expansion	Measure the outer radius
		Table top failed to stop	Adding lubrication	Measure dimensions after durability test
		Damage of hinge and table	Manufacturing control measures	Visual inspection of component
	Permanent damage of the hinge (damage of parts of shaft)	Functioning is compromised, total hinge failure	Manufacturing control measures	Visual inspection of component
Shaft	Failure by torsional yielding	Functioning is compromised, total hinge failure	FEM analysis to design part	Loss of motion and visual inspection
	Slippage, loss of friction	Reduced torque	Add lubrication	Measure dimensions after durability test
		Table top failed to stop	Consider manufacturing tolerances during design	Physical measurement of dimensions
		Damage of hinge and table		
	Jammed shaft movement	Loss of movement, hence loss of functionality of table	Ensure lubrication, check material compatibility	Lack of movement, loss of movement.
	Squeaky sounds	Annoyed user, increased wear	Good lubrication spread	
Left/Right part	Screw rips out of wood	Damage of table, loss of movement	Preventing failure modes of shaft and part on shaft	Durability tests
	Shaft and part lose connection gradually	No torque from hinge	Design the connection with FOS, evaluate the shape of the connection	Visual inspection and testing.
Mid Part	Screw rips out of wood	Damage of table, loss of movement	Preventing failure modes of shaft and part on shaft	Durability tests
	Permanent damage of the hinge (damage of parts of shaft)	Functioning is compromised, total hinge failure	Manufacturing control measures	Visual inspection of component
	Integrity failure	Functioning is compromised, reduced hinge life	Design with appropriate FOS Consider final specification for manufacturing for lifecycle assessment	Visual analysis/testing.

B Experimental data

B.1 Control Parameters

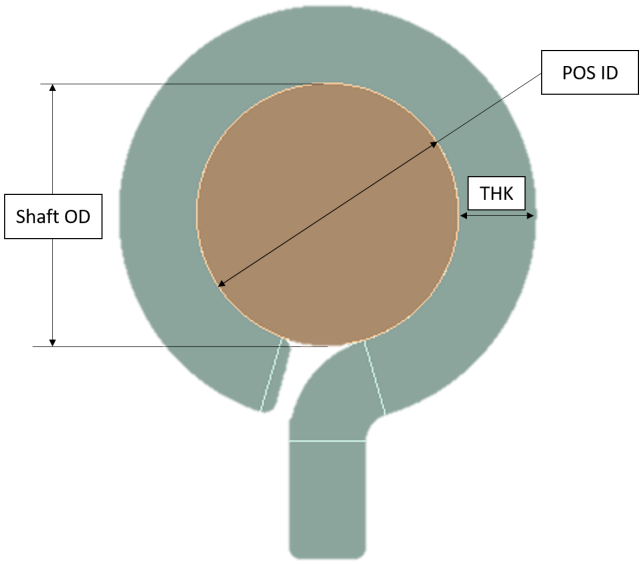

Figure B.1: *Figure showing the control parameters.*

[Experiment results have been excluded due to the intellectual property rights]

References

[1] H.-J. Bae. "Friction hinge device". US6467129B1. May 19, 2000.

[2] Z. Brzoska. "Tarcze kolowe i gruboscienne rury. (Polish) [Circular discs and thick-walled tubes]". *Wytrzymalosc Materialow. (Polish) [Strenght of Materials]*. Warsaw: Panstwowe Wydawnictwo Naukowe, 1972, pp. 307–326.

[3] L.-Y. Chiang, C.-S. Chu, and C.-Y. Lee. "Hinge with spacers". US2011232032A1. Mar. 26, 2010.

[4] L. Deters. "Tribology". *Springer Handbook of Mechanical Engineering*. Ed. by K.-H. Grote and E. K. Antonsson. Berlin, Heidelberg: Springer Berlin Heidelberg, 2009, pp. 295–326. ISBN: 978-3-540-30738-9. DOI: 10.1007/978-3-540-30738-9_5. URL: https://doi.org/10.1007/978-3-540-30738-9_5.

[5] E. Dragoni and A. Strozzi. Analysis of a split ring inserted into a circular housing. *Journal of Strain Analysis for Engineering Design* **21**.2 (1986), 59–70. ISSN: 03093247. URL: https://search.ebscohost.com/login.aspx?direct=true%5C&db=edo%5C&AN=ejs12218081%5C&site=eds-live%5C&scope=site%5C&authtype=guest%5C&custid=s3911979%5C&groupid=main%5C&profile=eds.

[6] ELESA S.p.A. *CMUF Hinges with adjustable friction*. 2021. URL: https://www.elesa.com/en/elesab2bstoreoc/Hinges-and-accessories--Hinges-with-adjustable--friction--CMUF-SR.

[7] Essentra plc. *Fixed Position Hinge*. 2021. URL: https://www.essentracomponents.com/en-gb/p/set-position-hinge-every-30-degree/498293.

[8] European Patent Office. *Espacenet Patent Search*. 2021. URL: https://worldwide.espacenet.com/.

[9] European Patent Office. *What is prior art?* 2015. URL: https://www.epo.org/learning/materials/inventors-handbook/novelty/prior-art.html.

[10] Fatigue behavior of Austenitic Type 316L Stainless Steel. *IOP Conf. Ser.: Mater. Sci. Eng. 36 012012* (2012). DOI: https://doi.org/10.1088/1757-899X/36/1/012012.

[11] D. M. Gannon. "Clip Friction Hinge". US56321895A. Nov. 27, 1995.

[12] M. Gelfand and E. T. Rude. "Improved Friction Hinge". WO9503464A1. July 22, 1993.

[13] Google. *Google Patents*. 2021. URL: https://patents.google.com/.

[14] K. Hanjalic et al. A robust near-wall elliptic-relaxation eddy-viscosity turbulence model for CFD. *Int. J. Heat Fluid Flow* **25** (2004), 1047–1051.

[15] Inter IKEA Systems B.V. *About us*. 2021. URL: https://about.ikea.com/en/about-us.

[16] Inter IKEA Systems B.V. *IKEA culture and values*. 2021. URL: https://about.ikea.com/en/about-us/ikea-culture-and-values.

[17] A. Iserles. *A First Course in the Numerical Analysis of Differential Equations*. Cambridge University Press, 2004. ISBN: 0-521-55655-4.

[19] J. Joseph E. Shigley; Charles R. Mischke; Thomas Hunter Brown. "FITS AND TOLERANCES". *Standard Handbook of Machine Design, Third Edition*. McGRAW-HILL, 2004, pp. 307–326. URL: https://www.accessengineeringlibrary.com/content/book/9780071441643/chapter/chapter27.

[20] J. A. Kossett. "Friction hinge system". US8875348B2. Aug. 30, 2013.

[21] P. M. Kurowski. *Finite Element Analysis for Design Engineers*. SAE International, Sept. 2004.

[22] C. Liao. "Free-positioning hinge". US20020144378A1. Jan. 10, 2002.

[23] D. A. Lowry and Y. Nokitov. "Hinge Assembly". US5491874A. June 20, 1993.

[24] S.-N. Lu. "Hinge Mechanism". US5950281A. July 16, 1998.

[25] V. C. Luppert. *Friction-hinge*. US761517A, March 1904.

[26] *MATLAB manual. Ordinary Differential Equations*. Version 7.8. Mathworks, 2008. URL: http://www.mathworks.com/access/helpdesk/help/techdoc/ref/ode45.html.

[27] *Mechanical User's Guide*. English. Version 2021 R1. ANSYS, Inc. 2021.

[29] J. Qiu and M. Zhou. Analytical Solution for Interference Fit for Multi-Layer Thick-Walled Cylinders and the Application in Crankshaft Bearing Design. *Applied Sciences* **6**.6 (2016). ISSN: 2076-3417. DOI: 10.3390/app6060167. URL: https://www.mdpi.com/2076-3417/6/6/167.

[30] Reell Precision Manufacturing Corporation. *Torque Engine Technologies*. 2013. URL: http://www.frictionhinge.com/tech.html.

[31] REELL PRECISION MANUFACTURING, INC. *PHCS*. 2021. URL: https://reell.com/products/position-hinges/phcs.

[32] Sierra Pacific Engineering & Products. *FH010SS, Adjustable Friction Hinge*. 2020. URL: https://spep.com/item/products/hinges/friction/sku-fh010ss/.

[33] S. R. Singiresu. *The Finite Element Method in Engineering*. Elsevier Science & Technology, 2004.

[34] Sugatsune America, Inc. *HG-TA45R TORQUE HINGE*. 2021. URL: https://www.sugatsune.com/product/torque-hinge-13/.
[35] D. Wahlstedt. "Clip friction hinge with housing". US6530123B1. Apr. 17, 2001.
[36] e. a. Zienkiewicz Olek C. *he Finite Element Method: Its Basis and Fundamentals : Its Basis and Fundamentals*. Elsevier Science & Technology, 2013.

DEPARTMENT OF MECHANICS AND MARITIME SCIENCES
CHALMERS UNIVERSITY OF TECHNOLOGY
Gothenburg, Sweden 2021
www.chalmers.se

CHALMERS
UNIVERSITY OF TECHNOLOGY